Biodegradable Polymer Nanocomposites: A Review of Properties

Hani Nasser Abdelhamid [a,b,c*]

[a]Advanced Multifunctional Materials Laboratory, Department of Chemistry, Faculty of Science, Assiut University, Assiut 71516, Egypt
[b]Proteomics Laboratory for Clinical Research and Materials Science, Department of Chemistry, Assiut University, Assiut, 71516, Egypt
[c]Nanotechnology Research Centre (NTRC), The British University in Egypt, El-Shorouk City, Suez Desert Road, P.O. Box 43, Cairo 11837, Egypt
*Corresponding authors: hany.abdelhamid@aun.edu.eg; hani.nasser@bue.edu.eg (Abdelhamid)

Abstract

Biodegradable polymers exhibit shortcomings, including low thermal stability and electrical conductivity. These challenges limit the broad applications of several applications, such as electronic devices. They show suitable dielectric, thermal, and electrical conductivity compared to the biodegradable polymer alone. Several methods can improve biodegradable polymers' dielectric, thermal, and electric conductivity, including co-polymerization, blending, and cross-linking with other polymers. Furthermore, the formation of nanocomposites seems to be the most effective method to improve the properties and performance of biodegradable polymers. This book chapter summarized biodegradable polymers' dielectric, thermal, and electrical conductivity. Biodegradable polymers nanocomposites consisting of polymers blend, inorganic, and other nanomaterials were discussed.

Keywords: Biodegradable polymers; Thermal conductivity; Dielectric; Nanocomposites.

1. Introduction

Polymers are multifunctional materials that can be alternatives to other materials such as metals, glass, and other traditional materials [1–5]. They can be pure organic [6–9] or hybrid materials including coordination polymers or metal-organic frameworks (MOFs) [10,11,20,12–19]. They offered various advantages such as being lightweight, flexible, and low cost. They are widely used for applications including electromagnetic interference shielding, biosensors, transient electronics skin (wearable) [21,22], wound dressings [23,24], tissue engineering [25], bone tissue scaffolds [26], self-healing strain sensor [27], sensors [28–30], optoelectronics [31], biomedicine[32–34], biotechnology [35–47], gene-delivery[48,49], environmental[50–58], and energy [11,16,56,58–71]. Polymers, including organic and coordination, are promising for future applications. In 1980, the term biodegradable polymers were introduced. Biodegradable polymers are widely applied for tissue engineering. Biodegradable polymers can be degraded into carbon dioxide (CO_2), water, biomass, and humus (dark organic matter in soil) using living organisms, photocatalysis, or catalysis. Biodegradation in a natural system is biologically benign using microorganisms or enzymes. The European standard of EN 13432 defined biodegradable materials as materials that can be degraded > 90% of their mass via biological environment for six months.

We introduce biodegradable polymers and the development of polymers nanocomposites. Here, we discuss biodegradable polymer nanocomposites' dielectric, thermal, and electrical conductivity. The synthesis of polymer nanocomposites exhibits high electric and thermal conductivity with good dielectric properties. The properties of polymers can be improved via conjugation with inorganic and organic materials.

2. Biodegradable polymers

The term “biodegradable” ensures products' reliability in the environment without harmful effects. The ASTM (e.g., ASTM D5511-18 and ASTM D5526-18, American Society for Testing and Materials) defined biodegradable materials as materials that exhibited 70% degradation during 30 days under anaerobic conditions[72,73]. Under aerobic conditions, ASTM D6400-19 and ASTM D6868-19 require 90% mineralization degradation of the material into CO_2 within 180 days[74,75]. Biodegradable polymers can be synthesized or extracted from different sources (**Figure 1**). They can be obtained from agro-resource biomass (i.e., agro-polymers). They can be extracted from microorganisms. They can be obtained from the conventional synthesis of bio-derived monomers. Petrochemicals are important sources of

monomers used for the synthesis of degradable polymers. They can be classified as (**Figure 1**):-

(1) Natural-based materials, e.g., polysaccharides (e.g., cellulose, lignin, starch, chitin/chitosan) or proteins (e.g., collagen, Silk fibril (SF)).

(2) Synthetic polymers, fossil oil, or petroleum-derived polymers e.g., poly(ε-caprolactone) (PCL) poly(lacticacid) (PLA), poly(butylenesuccinate), poly(glycolic acid) (PGA), poly(ε-caprolactone) (PCL), Poly(vinyl alcohol) (PVA), Poly(vinylpyrrolidone) (PVP), polybutylene succinate (PBS), and poly(hydroxyl butyrate) (PHB)[76–78].

Natural polymers can be classified as polysaccharides, polyamides, and polynucleotides (**Figure 1**). They can also be listed as plant-based polysaccharides (e.g., cellulose, alginate, or starch) and animal-derived polymers (e.g., collagen, silk fibroin, or chitosan). They exhibit advantages, such as high biocompatibility, low toxicity, low cost, good mechanical properties, and high biodegradability. Several linkages ensure high biodegradability (**Figure 2**).

Cellulose has been considered the most abundant biopolymer in nature (**Figure 2**)[65,79–87]. It is a linear polysaccharide biopolymer consisting of β-1,4-linked D-glucose units. It can be extracted from several sources, such as trees and cotton. The chemical structure of cellulose shows a large number of hydroxyl (–OH) groups[88]. Cellulose can proceed into the nanoscale, such as nanofibers (CNFs) and nanocrystals (CNCs).

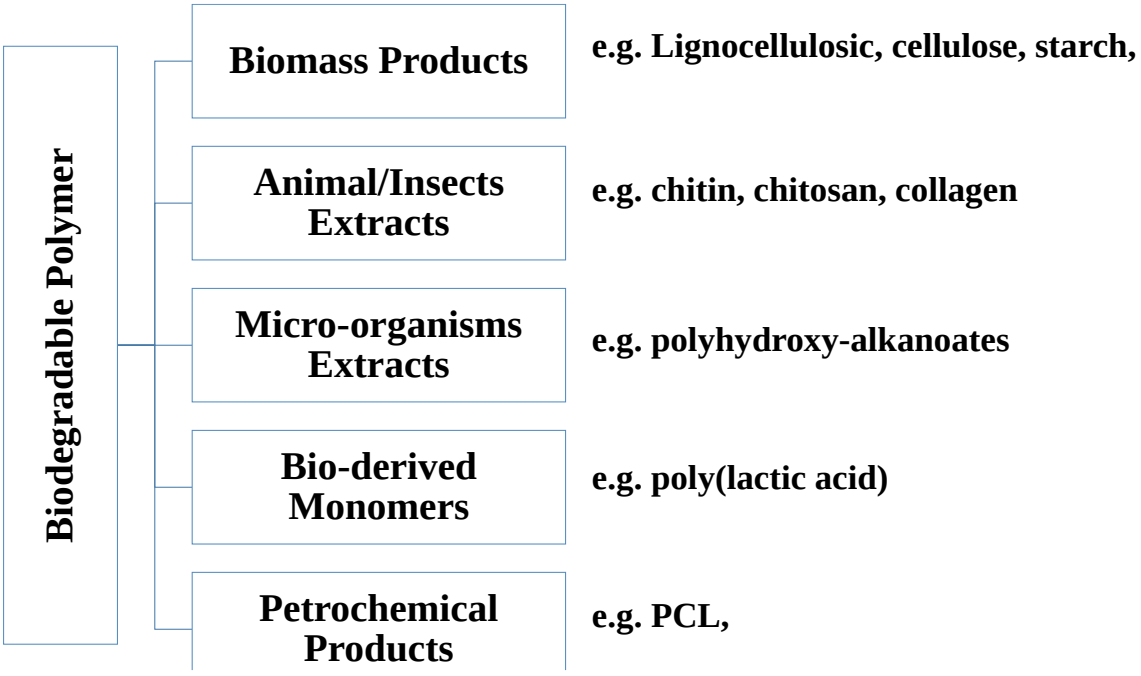

Figure 1. Biodegradable polymer sources.

Chitosan consists of randomly distributed β-(1-4)-linked D-glucosamine and N-acetyl-d-glucosamine[89–91]. It is the de-acetylated form of chitin offering amino groups. It can be dissolved in an acidic solution forming a cationic polysaccharide. It exhibits good adhesive properties with high antibacterial activity.

Synthetic polymers are usually extracted or synthesized via well-known reactions such as condensation or ring-opening polymerization (ROP). Several synthesis methods were reported for the synthesis of new organic polymers. Most of these methods require the use of a catalyst. The synthesis procedures aim to polymerize monomers with suitable functional groups that tend to polymerization. There are three main steps for polymerization: initiation, propagation, and termination. MOFs are coordination polymer formed via self-asselmbly of metal ions and organic linkers [64,66,69,92–98]. They can be decomposed into their constituent in harsh consition i.e. acid or base dpending on the MOFs materials.

Aliphatic polyester polylactide (PLA can be synthesized via ROP reaction of lactide using a catalyst such as tin (II) octoate. It can also be prepared via the condensation of lactic acid. It can also be extracted from corn or wheat. It displays good transparency with thermoplastic properties. It can be considered bioplastic. It is an everyday use for three-dimensional printing (3D printing)[78]. It can be degraded via hydrolysis, thermal decomposition, or photodegradation.

Like PLA, PCL can be obtained by ROP of ε-caprolactone [26]. United States Food and Drug Administration (US-FDA) approved PCL for biomedical applications such as tissue engineering. PCL exhibits high biocompatibility, high biodegradability, good chemical resistance, and high ductility. It displays a melting point of 65 °C with tunable viscosity enabling processing using several methods. However, it has high Young's modulus and strength.

A water-soluble polymer such as PVA can be synthesized via hydrolysis poly(vinyl acetate)[99]. It exhibits high transparency, high strength, good flexibility, and high biocompatibility. However, it has a high density of –OH groups; it is hard to shape via conventional processes such as melting methods. However, it can be easily blended with other materials via a mixing procedure. PVA–based materials were widely used for resistance random access memory [100–102]. PVP is another water-soluble polymer. It can be synthesized via the radical polymerization of N-vinylpyrrolidone [103]. PVP displays high

chemical resistance, easy processability, high transparency, good biocompatibility, and low cost. PVP was used for several applications, such as wearable electronic devices and gas sensors[104].

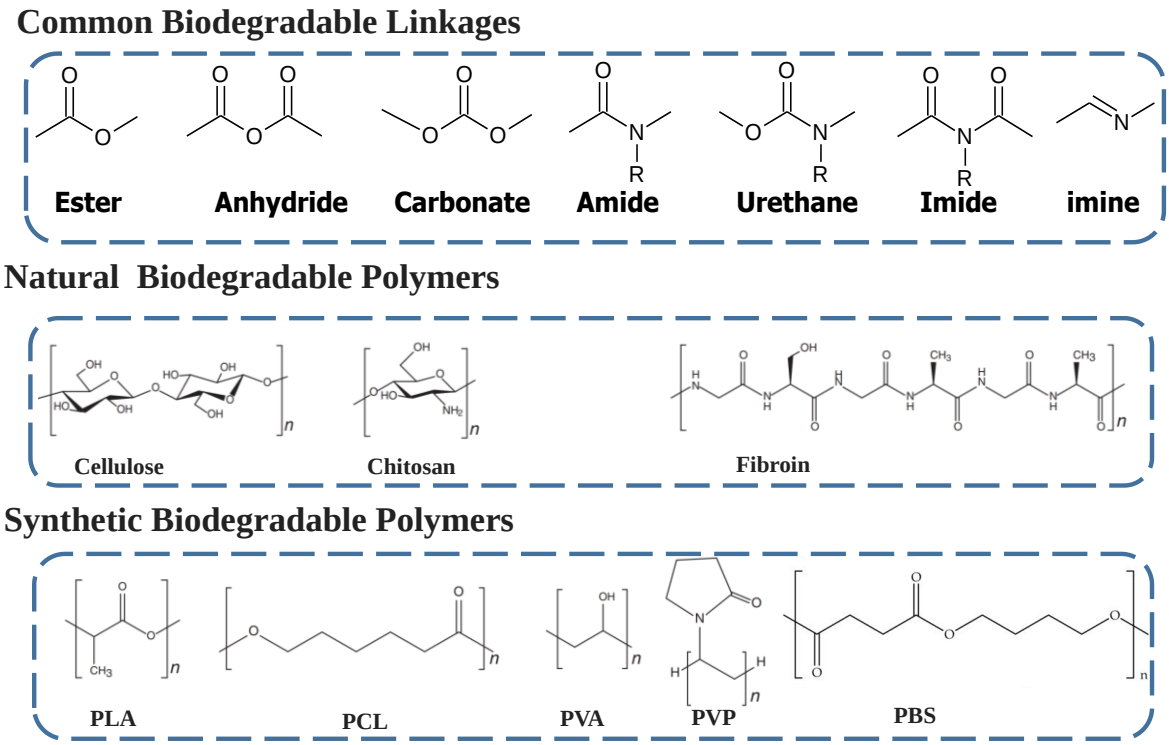

Figure 2 Common biodegradable linkage and chemical structure for common biodegradable polymers.

Natural polymers exhibit good intrinsic biocompatibility and enzymatic degradability, enabling intensive applications for biomedical applications (**Figure 2**). Biodegradable polymers are common clinical polymers, including polyglycolide, polylactides, and polycaprolactone. They can be classified as molecular, microstructural, and macroscopic. The properties of biodegradable polymers can be evaluated using UV–Vis spectroscopy, mass loss profiles, mass spectrometry, nuclear magnetic resonance (NMR), Fourier transform infrared (FT-IR) spectroscopy, Gel permeation chromatography (GPC), scanning electron microscopy (SEM), transmission electron microscopy (TEM), and atomic force microscopy (AFM).

The properties of polymers depend on several parameters, including chemical composition, particle size, morphology, and surface structure. Small particles polymers undergo aggregation into bulk materials, especially without proper stabilization. Nanoscale polymers have high

surface energy pushing the materials to aggregate to achieve high stability. Distributing the polymers uniformly in matrices can reduce or prevent the assembly.

The size of a polymer affects the properties of polymers. The morphology of the polymers can be spherical, rode, or plate, depending on the radius (R) and the thickness (t, **Figure 3**). Therefore, the ratio between volumes of interface material to the volume of the particle ($V_{interface}/V_{particle}$) increases with the decrease of particle size. The aspect ratio (the ratio of the diameter (2r) to the length (L)) determines the morphology of the polymers. Based on the aspect ratio, the morphology can be a plate, sphere, and rod with an aspect ratio of < 1, 1, and >1, respectively (**Figure 3**).

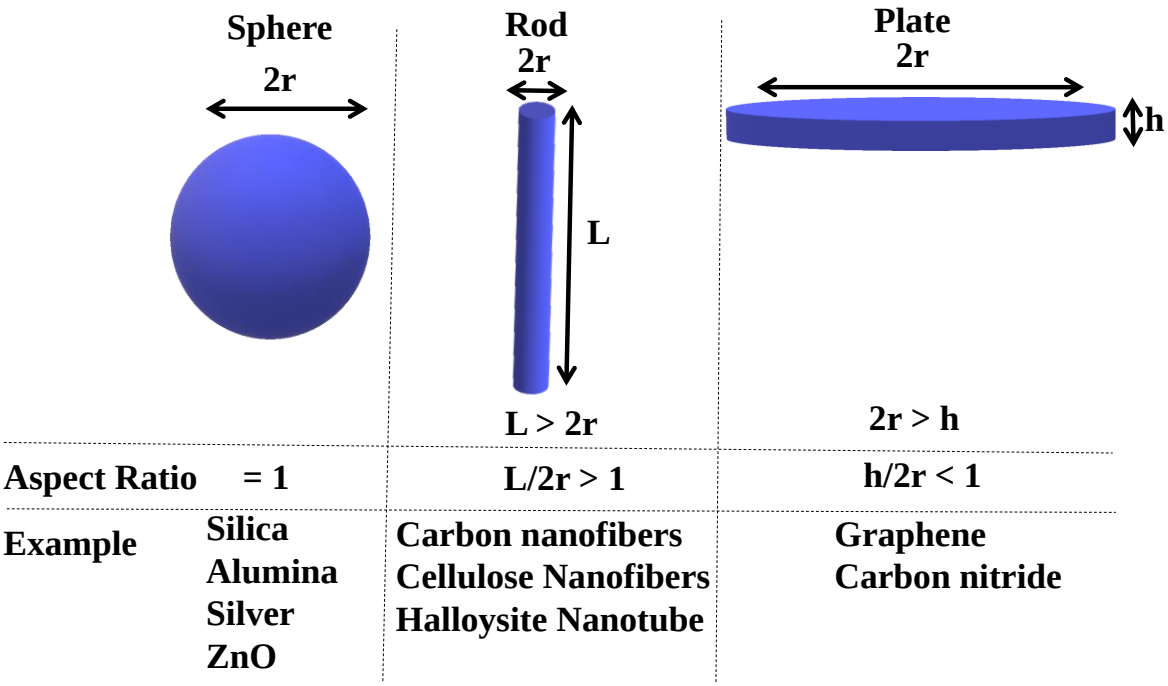

Figure 3. The morphology of polymers particles and their aspect ratio. R is the radius, L is length, and h is the height.

3. Polymers nanocomposites

The properties of the polymer can be significantly improved via several methods, including the addition of nanoparticles, i.e., the formation of nanocomposites. Polymers can be conjugated or blended with other materials to form composites. They can be conjugated with nanomaterials to form polymer nanocomposite (**Figure 4**). Polymer nanocomposites can generally be achieved using several methods such as:-

(a) Solution method: this method depends on the dissolution in a suitable solvent in the presence of nanoparticles followed by evaporation of solvent or via precipitation.
(b) Melt mixing: this method depends on the direct melt-mixed of polymer with the nanoparticle.

(c) In-situ polymerization: this method involves the polymerization of monomers without nanoparticles.

(d) Template synthesis: this method relies on using a template to synthesize nanoparticles.

Polymer nanocomposites (PNCs) are multiphase materials made of two or more materials containing a polymer and other materials, e.g., metal, ceramic, inorganic, non-metallic, and ionic liquids[105]. PNCs exhibit good physicochemical properties compared to individual components (**Figure 4**). Polymers nanocomposites are prepared via physical blending, dipping coating, casting, template molding, melt blending, mixing (via ultrasonication, shear, three-roll milling, ball milling), double-screw extrusion, and in-situ synthesis. Electro-hydrodynamic (EHD) method [106].

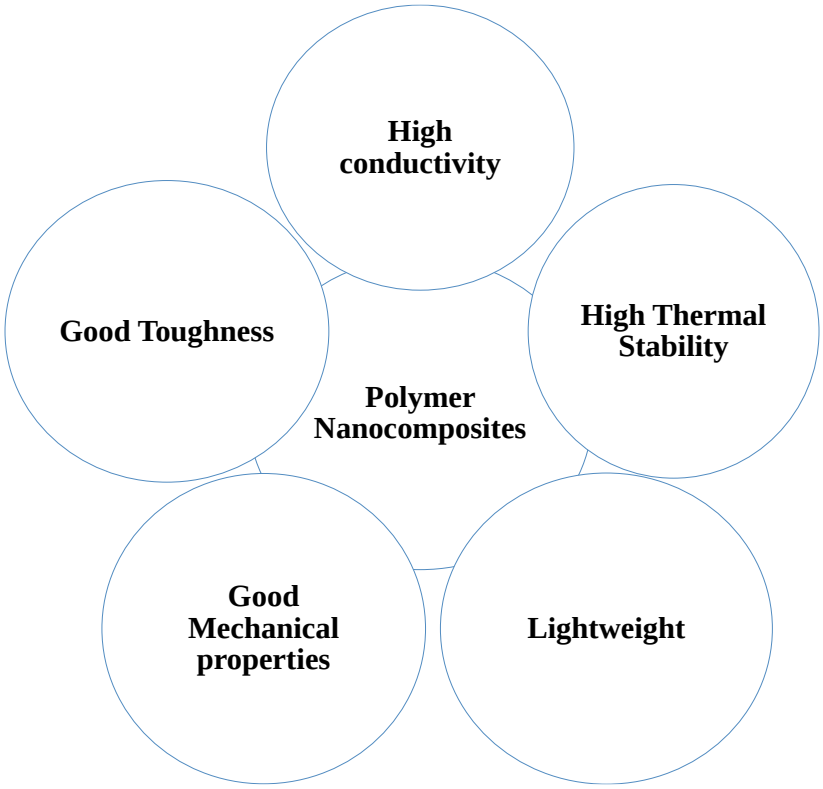

Figure 4. Advantages of polymer nanocomposite.

4. Dielectric Properties

The electrical insulator materials that can be polarized under an applied electric field are called dielectric materials. This material exhibits high electrical polarizability due to the accumulation of the electric charges on the dielectric materials under an electric field. The materials are insulators; thus, no flow of the electric charges can be performed through the material. The dielectric materials are not loosely bound or free, causing dielectric polarization that offers positive charges in the field's direction and negative charges that shift opposite the electric field. The material performance determines by a dielectric constant (*k*) that defines the material's storage capacity for the electrical charge. Materials with high-*k* values can be used as gate dielectrics in metal–oxide–silicon (MOS) transistors, memory cells, and supercapacitors. On the other hand, materials with low-*k* values are essential as electrical insulators.

The dielectric properties of polymers enable their applications for electronic skins (e-skins), capacitors, and dielectric resonator. A parallel plate capacitor exhibits a capacitance (*C*), defined as the ability to store a charge. The capacitance can be determined via the equation of $C = \varepsilon A/d$, where ε, A, and d are the dielectric constant, the area, and the space between the two electrodes, respectively. A dielectric layer of polymer is sandwiched between the two electrodes. The dielectric properties depend on several parameters such as composition, size, porosity, thin-film thickness, defects, operating frequency, doping concentration, and atomic number[31].

Ion-gel of cellulose can be used as dielectric materials [107]. Cellulose such as CNC was reported as a flexible field-effect transistor (FET) [108]. CNC can serve as substrate and dielectric materials. However, cellulose-based devices need a large operating voltage. The performance of cellulose can be improved via several methods, including mixing cellulose derivatives such as cyanoethyl cellulose-containing barium strontium titanate (BST, $Ba_xSr_{1-x}TiO_3$) nanoparticles[109]. The materials exhibit high dielectric properties, making them suitable for preparing ultralow-power electronics with a high on/off ratio and low operating voltage.

The thin film consisting of chitosan and Y_2O_3 nanoparticles exhibits a low current leakage current compared to pure chitosan. The electric and dielectric performance of chitosan can be improved via the impregnation of a high-K material (i.e., high dielectric constant)[40]. Similarly, silver nanoparticles (Ag NPs)/chitosan composite was used as a dielectric gate for

transparent resistive switching memory [110]. The composite offered high biocompatibility and required low-power operation conditions [110].

PVA has a dielectric constant of 5–8 in the 10–106 Hz range. It exhibits a higher dielectric constant than other biodegradable polymers [111,112]. An aqueous solution of PVA can be mixed with inorganic fillers materials such as Au NPs/graphene oxide (GO) [113], GO [114], and MoS_2 [115]. Inorganic nanoparticles improved the dielectric constant and strength of PVA films. A composite film of biodegradable poly(butylene succinate) and graphite exhibited a K-value of 113, which was 28 times higher than the pristine polymer matrix [116].

Various dielectric materials were mixed with biodegradable polymers such as PLA for electronic devices. PLA/TiO_2 was reported for the humidity sensor [117]. It can be used for the detection of humidity in the range of 20-90% [117]. PLA/barium titanate ($BaTiO_3$) nanowires (NWs) produce printable energy harvesters that can proceed using the 3D printing method [118]. $BaTiO_3$ nanowires can be well aligned, offering 273% higher power generation capacity than conventional cast nanocomposites with randomly oriented nanowires. Al_2O_3 improved the dielectric properties of cellulose acetate [119]. 3D printing was also reported for PLA/NiTi nanowires [120]. PLA/NiTi nanowires were reported as a sensor for measuring temperature and strain simultaneously [120]. Electrospinning of PLA/boron dye was reported to detect oxygen in real-time for tissue scaffold applications [121]. PLA/boron dye sensor can determine the low level of dissolved oxygen (< 15 ppm) in the scaffold [121]. Other materials, including cellulose nanocrystals (CNC)[122], clays [123], ZnO [124], SnO_2 [125], cobalt ferrites [126], nitride nanosheets /copper calcium titanate [127], gold nanoparticles [128], or PbS [129] were also reported to improve the dielectric properties of polymers. There are several mechanism for the dielectric improvement using these nanoparticles including the decrease in energy band gap [125].

Carbon nanomaterials such as carbon nanotubes improved the dielectric properties of commercially available polymers, Ecoflex® [130]. It was found that there is an increase in the dielectric value with the rise of the carbon nanotube's contents. Reduced graphene oxide (rGO) improved the dielectric properties of polyaniline (PANI)/calcium copper titanate ($CaCu_3Ti_4O_{12}$) [131]. It can be also improved PVP-PVA [132], and starch [133].

5. Thermal Properties

The thermal properties of polymers can be determined using several analytical techniques such as thermogravimetric analysis (TGA), differential thermal analysis (DTA), and differential

scanning calorimetry (DSC). TGA can be connected with other analytical instruments to characterize degradable production, such as TGA\FT-IR spectroscopy.

A composite of silica/carbon exhibited the thermal properties of biodegradable and commercial polymer Ecoflex (a blend of L,D-polylactide (L,D-PLA) and PCL) [134]. DSC analysis indicated an improvement in the composite's glass transition temperature (T_g) and crystallization temperature. There is an enhancement of decomposition onset and maximum temperatures by 15 °C and 16 °C, respectively. The thermal improvement is due to increased cross-linking caused due to the inorganic nanoparticles [134]. Carbon nanomaterials such as CNT enhanced the T_m of PLA [135]. CNC improved the thermal stability of polyaniline (PANI) [136].

The coordination of Cd^{2+} ions with chitosan improved the thermal stability of chitosan [137–139]. The presence of CdS quantum dots enhanced the thermal stability of chitosan. The thermal decomposition of CdS/chitosan was increased by 60 °C compared to pure chitosan [137,138,140–142]. Co-doped ZnO improved thermal stability of carboxymethyl cellulose (CMC)[143].

TGA and TGA-FTIR were used to characterize PCL and PLA's thermal stability and degradation [144]. Data analysis showed that PCL exhibited higher thermal stability than PLA. However, PLA has higher activation energy showing higher degradation kinetics. This observation indicates that the degradation rate depends on temperature. A blend of PLA and PCL showed lower thermal stabilities than both polymers. However, the thermal stability can be improved by adding TiO_2 nanoparticles[144]. TiO_2 NPs also improved the thermal stability of PLA/poly(hydroxybutyrate-co-valerate) (PHBV) [145].

Thermal analysis of pure PCL and PCL: lithium thiocyanate (LiSCN) salt complexes using different compositions were reported (**Figure 5**) [146]. DSC thermogram for pure PCL showed a relatively sharp endothermic peak at 64 °C. This observation indicates the high purity of the PCL. However, DSC thermograms of the PCL\LiSCN composite showed a shifting in the melting temperature (Tm) toward lower temperatures with increased LiSCN contents. The drop of Tm in the presence of the salt addition is due to the decrease in size and free energy (**Figure 5**).

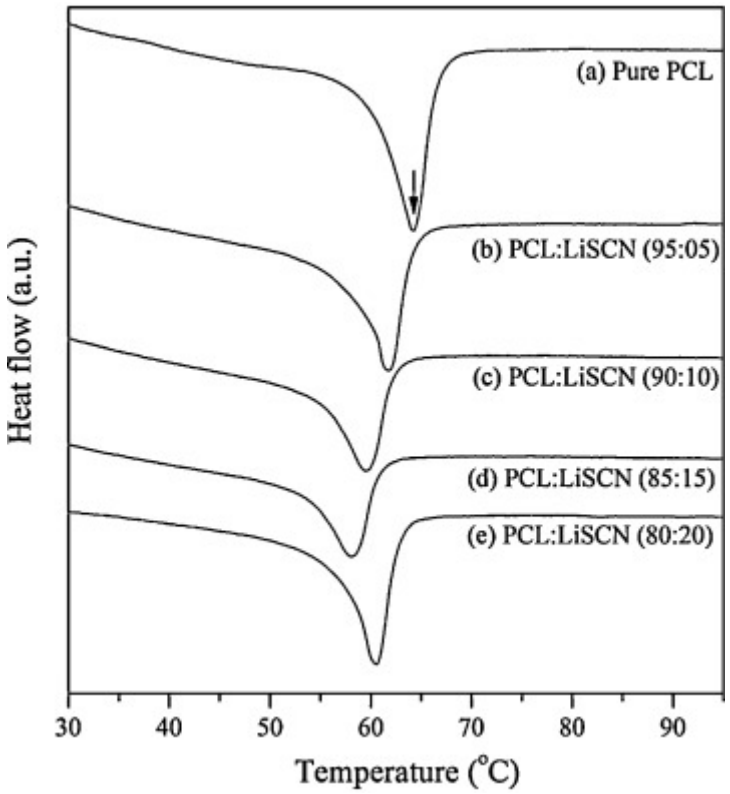

Figure 5 DSC analysis of PCL:LiSCN films embedded different concentrations of LiSCN [146]. *Copyright 2015. Reproduced with permission from Elsevier.*

6. Thermal Conductivity for Biodegradable Polymer Nanocomposites

Thermal conductivity is the ability to conduct heat. Thermal conductivity is measured in watts per meter kelvin ($W^{-1}•m^{-1}•K^{-1}$) according to the International System of Units (SI). Organic polymers are heat insulators with low thermal conductivity (TC, 0.2 $W^{-1}•m^{-1}•K^{-1}$). The low TC values of polymers hinder their adoption in electronic applications. The TC of polymers can be improved via several methods, including synthesizing polymers nanocomposites with organic and inorganic materials.

A solvent-free spherical cellulose nanocrystals fluids (CNCfs) embedded PLA membrane was fabricated using electrospinning [147]. PLA/CNCfs fibrous membrane exhibited high thermal conductivity of 0.27 $W^{-1}•m^{-1}•K^{-1}$[147]. A melt extrusion-stretching method was reported to process a biodegradable composite of PLA/poly(butylene adipate-co-butylene terephthalate)/carbon nanofiber (PLA/PBAT/CNF) [148]. PLA/PBAT/CNF containing CNF of 10 wt.% exhibited in-plane TC of 1.53 $W^{-1}•m^{-1}•K^{-1}$. CNF offered a 31.9% increment in the thermal conductivity of the biocomposite[148].

Hydroxyl-functionalized hexagonal boron nitride (OH-h-BN) nanoplatelets improved thermal conductivity for chitosan microspheres (CSM)[149]. OH-h-BN/CSM nanocomposites exhibit thermal conductivity of 5.66 $W•m^{-1}•K^{-1}$. It showed 502% and 1914% enhancement compared to OH-h-BN/CS nanocomposites and pure chitosan, respectively [149]. A simple and environmentally friendly strategy was reported to fabricate epoxy/BN composites[150]. The synthesis method improved the through-plane TC of the prepared composite. The effect of filler sizes of BN on thermal conductivity was also investigated. The data analysis showed that the high content of BN in the epoxy composite ensured a higher through-plane TC of 2.01 $W•m^{-1}•K^{-1}$ [150].

Metallic nanoparticles exhibit high thermal conductivity ensuring significant improvement for polymers nanocomposites. Metallic nanoparticles such as silver nanowires (Ag NWs) improved the through-plane thermal conductivity of cigarette filters (CF, non-biodegradable cellulose acetate), offering TC of 1.71 $W•m^{-1}•K^{-1}$ at the loading of 2.8 vol% Ag NWs[115]. A cellulose nanofibers/MXene@Ag film showed TC of 22.43 $W•m^{-1}•K^{-1}$ due to the synergistic effect of Ag NPs[116].

Carbon nanomaterials such as graphene improve the thermal conductivity of polymers. They have high TC at ambient temperature. Graphene exhibits a high aspect ratio with high TC ($\geq$5000 $W•m^{-1}•K^{-1}$)[151]. The TC value of epoxy (BE)/4,4′-diaminodiphenyl methane/GNP (graphite nanoplatelets) and BE/DDMGNP-10 nanocomposites was enhanced to 2.21 $W•m^{-1}•K^{-1}$ which is ten times higher than conventional EP [152]. Cellulose/multiwall carbon nanotube (MWCNT) exhibited in-plane and through-plane TC of 1.98 and 0.34 $W•m^{-1}•K^{-1}$, respectively [153]. The composite was prepared via several steps, including 1) a simple paper-making step, 2) a layer-by-layer assembly step, and 3) *in-situ* welding (**Figure** 6**A**). There is a significant increase in the in-plane TC with the addition of CNT content without a substantial increase in the through-plant conductivity (**Figure 6B**)[153]. MWCNT and GNP improved thermal and electrical conductivity for composites of polyoxymethylene (POM)/ PLA/MWCNT and POM/graphene nanoplate (GNP) (denoted as PMCNT and PMGNP, respectively)[154]. PMCNT and PMGNP exhibited electrical and through-plane thermal conductivities of 3484 $S•m^{-1}$ and 1.95 $W•m^{-1}•K^{-1}$, respectively, for PMCNT40, and 2695 $S•m^{-1}$ and 4.24 $W•m^{-1}•K^{-1}$, for the corresponding values for PMGNP48 [154]. MWCNT improved the thermal and electrical conductivity compared to GNPs. GNPs (loading of 40 wt.%) improved the thermal and electrical conductivity for the PBAT/PLA blend (ratio of PBAT:PLA was 75:25), offering thermal conductivity and electrical conductivity of 3.15

$W \bullet m^{-1} \bullet K^{-1}$ and 338 $S \bullet m^{-1}$, respectively[155]. The polymer's properties are enhanced with the GNPs content (**Figure** 7). The presence of PLA ensures a confined composite of PBAT and GNPs according to TEM images (**Figure** 7).

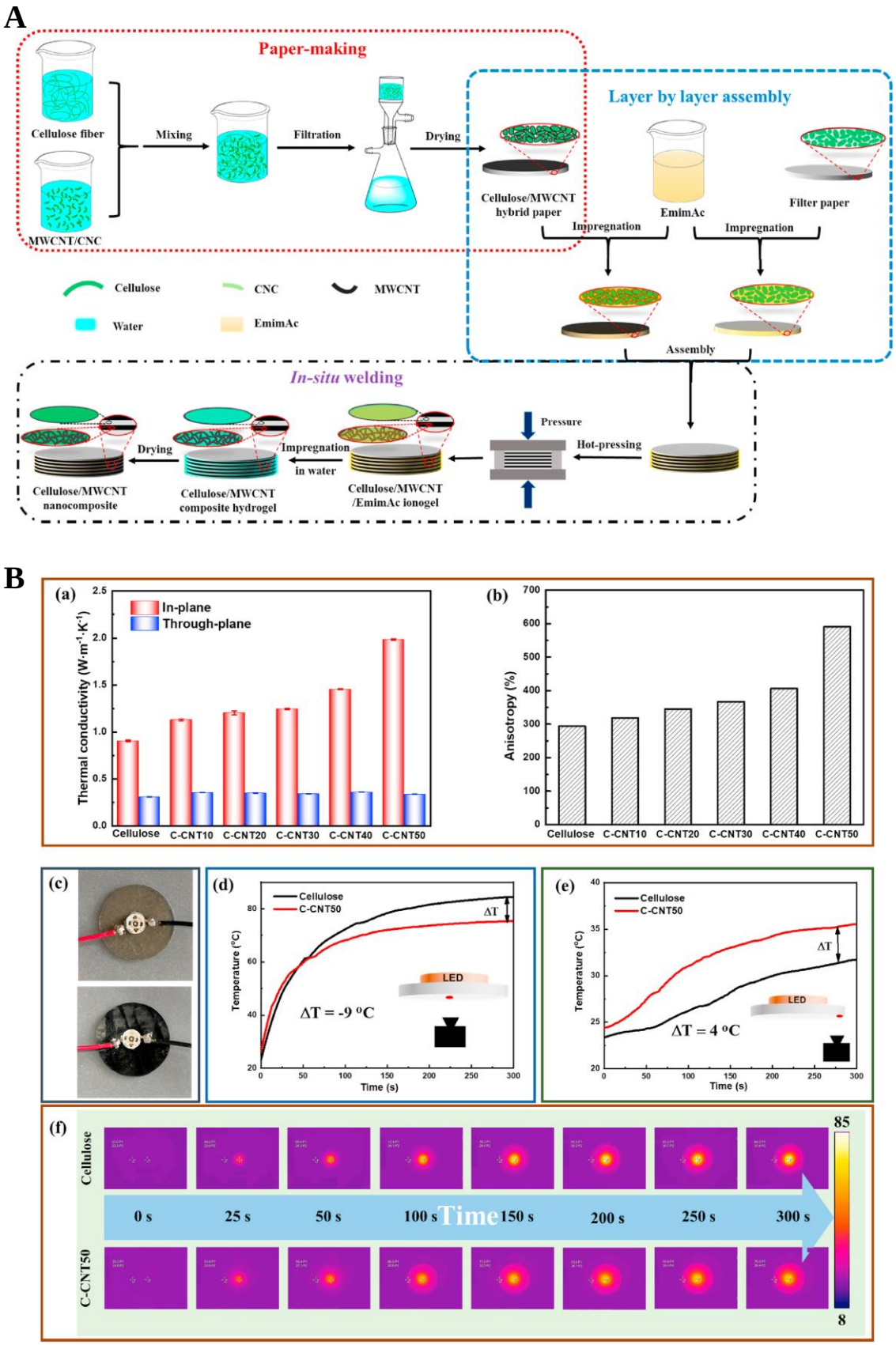

Figure 6 A) Schematic of the fabrication process of the cellulose/MWCNT nanocomposites, and B) a) TC and (b) TC anisotropy of cellulose/MWCNT nanocomposites, (c) Photographs

of cellulose (upper) and C-CNT50 (lower), (d) and (e) Surface temperature. (f) Infrared thermal images [153]. *Copyright 2021. Reproduced with permission from Elsevier.*

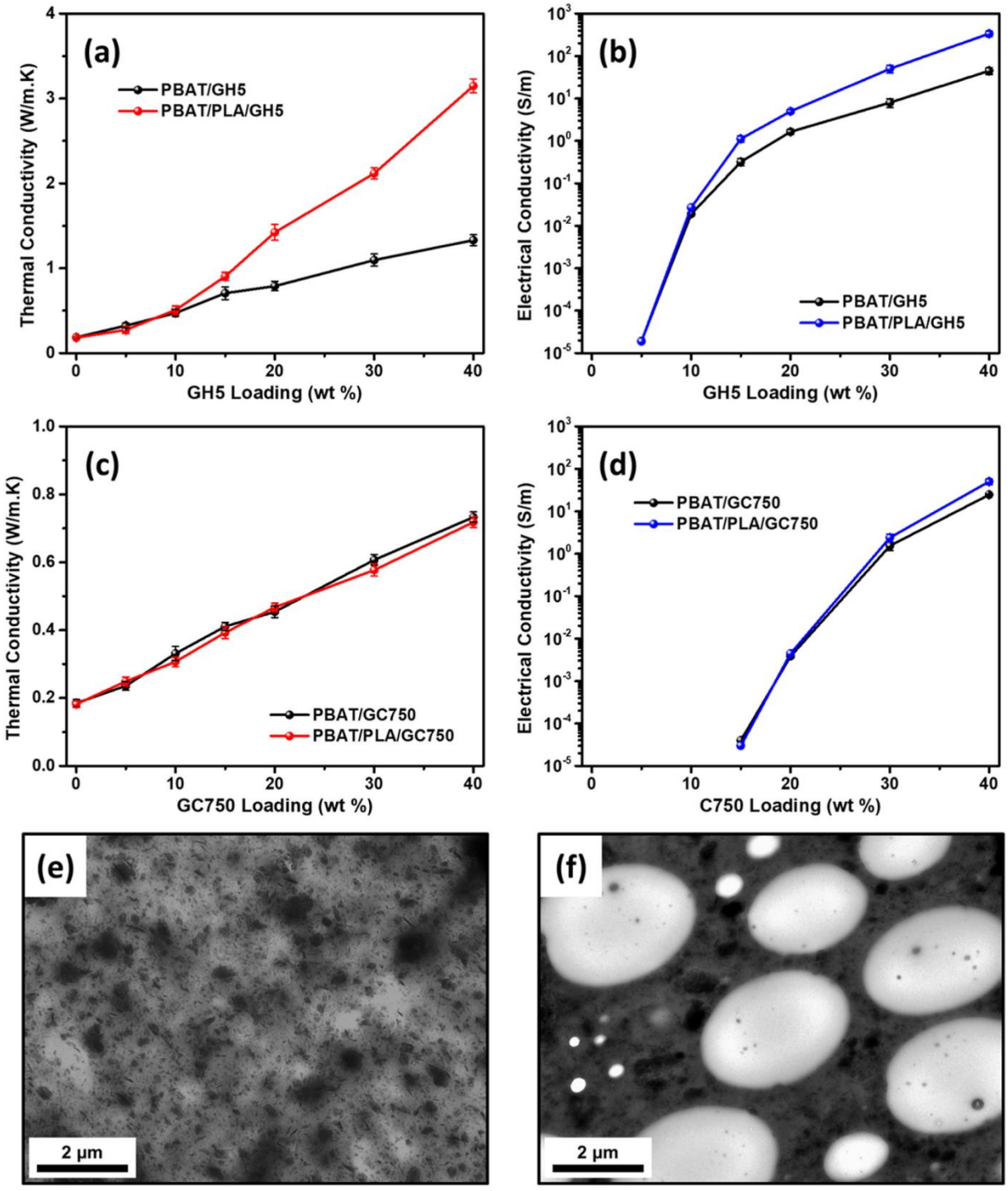

Figure 7 a, c) thermal conductivity, b, d) electrical conductivity, of a-b) PBAT/GNPs and c-d) PBAT/PLA/GNPs, e-f) TEM images of e) PBAT/GNPs, and f) PBAT/PLA/GNPs [155]. *Copyright 2020. Reproduced with permission from Elsevier.*

7. Electrical Conductivity

Electronic devices are usually used in traditional polymers such as polypropylene (PP), polystyrene (PS), polyimide (PI), and poly(ethylene terephthalate) (PET). These polymers are mainly non-degradable, causing environmental concerns. In contrast, biodegradable polymers are environmentally friendly with high biocompatibility and metabolization properties. Thus, they can be used for implantable chips and wearable devices.

Most reported polymers lack high conductivity except for some conducting polymers (CPs). The low conductivity of polymers is due to the covalent bonding. A strong bond, i.e., covalent bonds, prevents electron channels or ion migration. Compared with traditional conductive materials, CPs offer advantages, including high flexibility, lightweight, and low cost. CPs can be classified into two categories: Structural (intrinsic) structural CPs (SCPs): e.g., polyaniline (PANI), polypyrrole (PPy), polyphenyl acetylene (PPA), and their derivatives, and CPs composites (CPCs): incorporating the polymers with conductive fillers, e.g., carbon black (CB), carbon nanotubes (CNTs), and graphene (G).

Several critical parameters affect the polymer's conductivity (**Figure 8**). The size of polymers determines the polymer conductivity. When the volume fraction of polymers increases to a specific critical value, there is a significant increase in the conductivity of the polymer, i.e., conversion of insulator materials to the conductor. The conductivity of biodegradable polymers can be improved by adding conductive nanofillers. It can be improved by adding a small volume fraction of high conductivity materials. The conjugated polymers exhibit electrical conductivity in the range of 10^{-10} to 10^{-5} S•cm^{-1}. The electrical conductivity can be improved via several methods, including doping with molecules such as salt ions that can improve the polymer's electrical conductivity to 10^{4} S•cm^{-1}. As a rule of thumb, the critical value (defined as the percolation threshold) of the conductive material in the composites offers a significant increase of several orders of magnitude in conductivity. The critical value of the conductivity materials in polymer composite converts an insulator to a conductor. Above this threshold, the relation between the concentration and the conductivity (σ) or electrical resistivity (ρ) can be described by a scaling law[156]:

$$\sigma = \sigma_0[(\varphi - \varphi_c)]^t$$

$$\rho = \rho_0[(\varphi - \varphi_c)]^t$$

where σ_0, ρ_o, t, φ, and φ_c represent the intrinsic conductivity of the fillers, the resistivity coefficient, the exponent, the volume fraction of conductive particles, and percolation transition, respectively. The exponent t depends on the dimensionality of the polymers, which is called universal percolation behavior. Based on the theoretical calculation, it equals 1–1.3 and 2 for two-dimensional (2D) networks and a three-dimensional (3D) network.

Nanofiller materials exhibit higher electrical properties than microsized fillers. Conductive nanofillers with a large aspect ratio (e.g., CNTs, graphene) exhibited an excellent connected conductive network providing a low percolation threshold. The use of carbon nanomaterials such as graphene improved the thermal conductivity of the biodegradable polymers[157]. Chitosan composite film containing GO exhibits good proton conductivity. PBAT composite containing 40 wt.% of graphene nanoplatelets (GNPs) exhibited electrical and thermal conductivity of 3.15 $W \bullet m^{-1} \bullet K^{-1}$ and 338 $S \bullet m^{-1}$, respectively [155]. GNPs improved the electrical conductivity for PLA/chitosan (75/25 wt./wt.) [158], and polyhedral oligomeric silsesquioxane/PCL (POSS-PCL)[159]. The use of plasticizers such as glycerol improved the conductivity for poly(vinyl alcohol) (PVA) films and PVA/starch blend [160]. Data analysis reveals that there is an increase of the conductivity for PVA with the increase in the content of glycerol and starch [160]. The same observation was reported for Chitosan\$AgNO_3$\$Al_2O_3$ system using glycerol as a plasticizer [161].

The conductivity of PLA can be improved by incorporating gold nanoparticles (Au NPs)[162]. The PLA/Au NPs/indium tin oxide (ITO) electrode was used as an electrochemical biosensor for the selective identification of leukemia cancer cells [162]. Silver nanowires improved the conductivity of PLA [163]. PLA/Ag NPs were reported as electrodes for the organic light-emitting diodes (OLEDs) [163]. It offered high transparency with good electrical conductivity, even after 10 000 cycles[163]. AgNPs-Ni_2O_3 improved the electrical conductivity of cellulose nanowhiskers/polypyrrole [164]. Ag NPs can be also used to improve the electrical conductivity for chitosan [165].

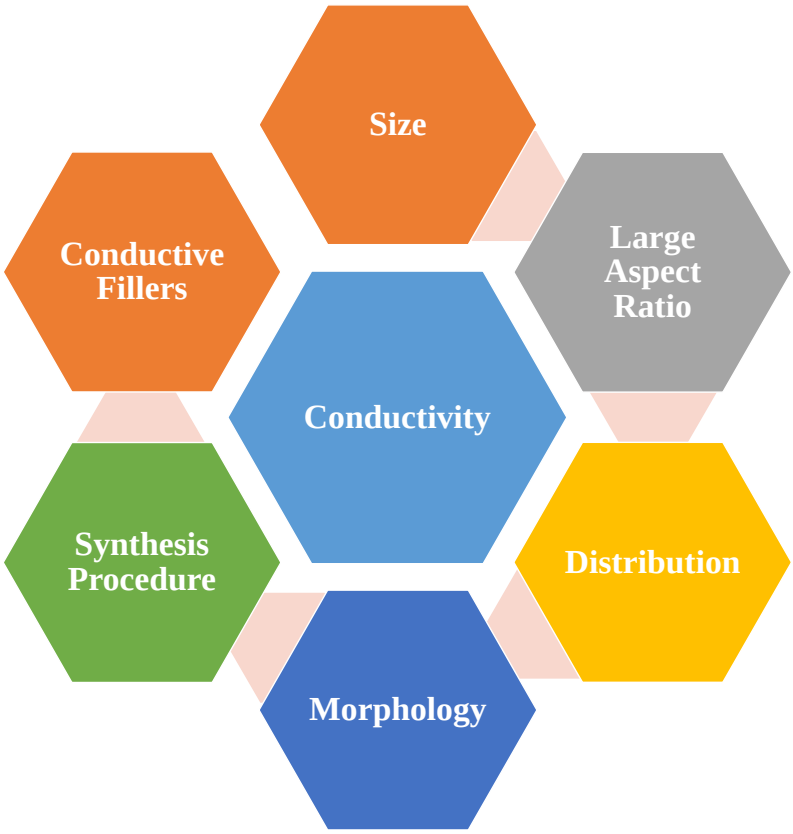

Figure 8. Key parameters are affecting polymer's conductivity.

The perfect interconnection between polymers and conductive nanofillers is critical for constructing a conductive nanocomposite. The homogenous distribution of nanofiller in the polymer nanocomposite improved the electrical conductivity of the composite. Naturally, the nanofillers tend to distribute randomly in the polymer matrix. It was reported that some fillers tend to spread to the polymer's surface at higher concentrations.

A study showed a correlation between the dispersion state of MWCNTs in PP and electrical conductivity [166]. The composite was synthesized using two different procedures; 1) chemical modification of MWCNTs and 2) incorporation of a master batch [polypropylene-grafted-maleic anhydride (PP-g-MA)] as a compatibilizer followed by a simple melt blending. Based on the optical microscopic images of MWCNTs/PP composite, the addition of a compatibilizer enhanced the uniform dispersion of MWCNTs in the PP matrix. Although it reduced the conductivity. However, the post-heat treatment improved the interconnection between MWCNTs and PP, leading to higher electrical conductivity. The uniform distribution and construction of a compelling relationship between the composite are crucial. Amphiphilic polymers prevent the aggregation in nanocomposites non-covalently attachment.

The addition of CNT improved the conductivity of several polymers, such as PCL[167,168], polypropylene (PP)[168], PLA[169], and chitosan-PCL[170]. The dispersion of conductive carbon nanoparticles (e.g., CB, CNTs) in PLA can be improved via the addition of ramie fiber (RF)/PLA, resulting in different sensing mechanisms [169]. PCL/CNTs nanocomposites were synthesized via in-situ grafting and polymerization of PCL and CNTs [171]. It exhibits good conductivity enabling quantitative sensing of organic vapors[171]. The melt-blown method synthesized PCL/PP/CNTs [168]. A 3 wt.% CNTs offered a significant high electrical resistance of the polymer nanocomposites, enabling the detection of various solvents[172]. PCL/CNTs/PLA blends containing four wt.% CNTs were synthesized via the melt-spun procedure as fibers[168]. The fibers exhibited good electrical properties for application as a textile sensor. CNTs\PCL composite can be used to monitor the temperature in a range of 20-80 °C [168]. MWCNT exhibited more remarkable POM/PLA composite improvement than GNPs (**Figure 9**)[154]. The conductivity depends on the loading of both materials (**Figure 9**)[154].

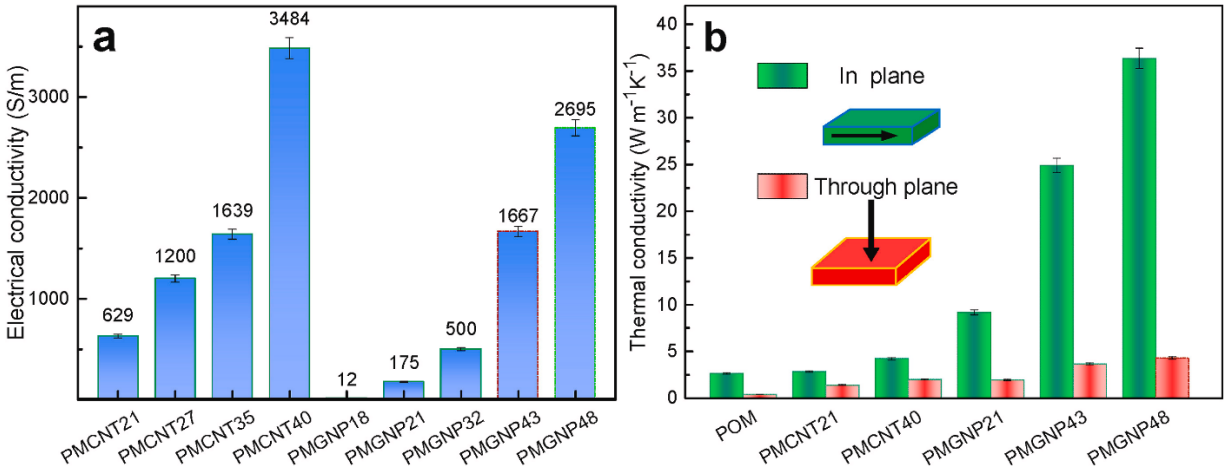

Figure 9. (a) Electrical and (d) thermal conductivity.[154] *Copyright 2021. Reproduced with permission from Elsevier.*

The nanofiller materials such as metallic nanoparticles or metal oxides with high conductivity ensure high conductivity. The electrical properties of PVA can be improved by adding In_2O_3/Cr_2O_3 nanoparticles [128] and GO [129]. 3D printing PVA/GO devices can be operated in a small gate voltage range of −0.5 to 2.5 V for electronic devices and circuits[129]. Graphite/diamond particles [173] and G [174] enhanced the electroconductive of PLA nanocomposites. Nano-clay improved the electrical conductivity of bacterial cellulose (BC)\PANI to 0.49 $S•cm^{-1}$ using only 5 wt.% of the clay [175]. It exhibited 16 folds improvement in the electrical conductivity for the polymer blend [175]. The improvement in the conductivity of biodegradable polymers enable the fabrication of energy storage devices with high biodegradability [176].

8. Conclusions

This chapter discusses the dielectric, thermal, and electrical conductivity properties of biodegradable polymers nanocomposites. The fabrication process of biodegradable polymer nanocomposite can significantly influence the electrical properties. There are several methods for the synthesis and fabrication of polymer nanocomposites. However, preparing nanocomposite with high conductivity, i.e., low percolation threshold, remains challenging. There is a lack of clear procedures to characterize biodegradable polymers' dielectric, thermal, and conductivity. Potentially, there is high progress in evaluating the material's properties to ensure high benefits.

9. References

[1] Zheng N, Xu Y, Zhao Q, Xie T. Dynamic Covalent Polymer Networks: A Molecular Platform for Designing Functions beyond Chemical Recycling and Self-Healing. Chem Rev 2021;121:1716–45. https://doi.org/10.1021/acs.chemrev.0c00938.

[2] Zhao X, Chen X, Yuk H, Lin S, Liu X, Parada G. Soft Materials by Design: Unconventional Polymer Networks Give Extreme Properties. Chem Rev 2021;121:4309–72. https://doi.org/10.1021/acs.chemrev.0c01088.

[3] Feng Q-K, Zhong S-L, Pei J-Y, Zhao Y, Zhang D-L, Liu D-F, et al. Recent Progress and Future Prospects on All-Organic Polymer Dielectrics for Energy Storage Capacitors. Chem Rev 2022;122:3820–78. https://doi.org/10.1021/acs.chemrev.1c00793.

[4] Yao Q, Bermejo Gómez A, Su J, Pascanu V, Yun Y, Zheng H, et al. Series of Highly Stable Isoreticular Lanthanide Metal–Organic Frameworks with Expanding Pore Size and Tunable Luminescent Properties. Chem Mater 2015;27:5332–9. https://doi.org/10.1021/acs.chemmater.5b01711.

[5] Abdelhamid HN, Huang Z, El-Zohry AM, Zheng H, Zou X. A Fast and Scalable Approach for Synthesis of Hierarchical Porous Zeolitic Imidazolate Frameworks and One-Pot Encapsulation of Target Molecules. Inorg Chem 2017;56:9139–46. https://doi.org/10.1021/acs.inorgchem.7b01191.

[6] Abdelhamid HN, Wu H-F. Polymer dots for quantifying the total hydrophobic pathogenic lysates in a single drop. Colloids Surfaces B Biointerfaces 2014;115:51–60. https://doi.org/10.1016/j.colsurfb.2013.11.013.

[7] Abdellah AR, El-Adasy A-BA, Atalla AA, Aly KI, Abdelhamid HN. Palladium nanocrystals-embedded covalent organic framework (Pd@COF) as efficient catalyst for Heck cross-coupling reaction. Microporous Mesoporous Mater 2022:111961. https://doi.org/10.1016/j.micromeso.2022.111961.

[8] Abdellah AR, El-Adasy A-BA, Atalla AA, Aly KI, Abdelhamid HN. Palladium nanocrystals-embedded covalent organic framework (Pd@COF) as efficient catalyst for Heck cross-coupling reaction. Microporous Mesoporous Mater 2022:111961. https://doi.org/10.1016/j.micromeso.2022.111961.

[9] Ibrahim M, Abdelhamid HN, Abuelftooh AM, Mohamed SG, Wen Z, Sun X. Covalent Organic Frameworks-Derived Nitrogen-Doped Carbon/Reduced Graphene Oxide as Electrodes for Supercapacitor. SSRN Electron J 2022. https://doi.org/10.2139/ssrn.4063571.

[10] Abdelhamid HN. Biointerface between ZIF-8 and biomolecules and their applications.

Biointerface Res Appl Chem 2021;11:8283–97. https://doi.org/10.33263/BRIAC 111.82838297.
[11] Abdelhamid HN. Salts Induced Formation of Hierarchical Porous ZIF-8 and Their Applications for CO2 Sorption and Hydrogen Generation via NaBH4 Hydrolysis. Macromol Chem Phys 2020;221:2000031. https://doi.org/10.1002/macp.202000031.
[12] Goda MN, Abdelhamid HN, Said AE-AA. Zirconium Oxide Sulfate-Carbon (ZrOSO4@C) Derived from Carbonized UiO-66 for Selective Production of Dimethyl Ether. ACS Appl Mater Interfaces 2020;12:646–53. https://doi.org/10.1021/acsami.9b17520.
[13] Abdelhamid HN. Surfactant assisted synthesis of hierarchical porous metal-organic frameworks nanosheets. Nanotechnology 2019;30:435601. https://doi.org/10.1088/1361-6528/ab30f6.
[14] Abdelhamid HN. Dehydrogenation of sodium borohydride using cobalt embedded zeolitic imidazolate frameworks. J Solid State Chem 2021;297:122034. https://doi.org/10.1016/j.jssc.2021.122034.
[15] Zulfajri M, Abdelhamid HN, Sudewi S, Dayalan S, Rasool A, Habib A, et al. Plant Part-Derived Carbon Dots for Biosensing. Biosensors 2020;10:68. https://doi.org/10.3390/bios10060068.
[16] Abdelhamid HN. UiO-66 as a catalyst for hydrogen production via the hydrolysis of sodium borohydride. Dalt Trans 2020;49:10851–7. https://doi.org/10.1039/D0DT01688H.
[17] Abdelhamid HN, Sharmoukh W. Intrinsic catalase-mimicking MOFzyme for sensitive detection of hydrogen peroxide and ferric ions. Microchem J 2021;163:105873. https://doi.org/10.1016/j.microc.2020.105873.
[18] Abdelhamid HN, Dowaidar M, Hällbrink M, Langel Ü. Cell Penetrating Peptides-Hierarchical Porous Zeolitic Imidazolate Frameworks Nanoparticles: An Efficient Gene Delivery Platform. SSRN Electron J 2019. https://doi.org/10.2139/ssrn.3435895.
[19] Sadek AA, Abd-Elkareem M, Abdelhamid HN, Moustafa S, Hussein K. Enhancement of critical-sized bone defect regeneration using UiO-66 nanomaterial in rabbit femurs. BMC Vet Res 2022;18:260. https://doi.org/10.1186/s12917-022-03347-9.
[20] Abdelhamid HN. Hierarchical Porous Zeolitic Imidazolate Frameworks: Microporous to Macroporous Regime, 2022, p. 431–47. https://doi.org/10.1007/978-3-030-85397-6_14.
[21] Peng X, Dong K, Wu Z, Wang J, Wang ZL. A review on emerging biodegradable polymers for environmentally benign transient electronic skins. J Mater Sci 2021;56:16765–89. https://doi.org/10.1007/s10853-021-06323-0.
[22] Emam HE, Abdelhamid HN, Abdelhameed RM. Self-cleaned photoluminescent viscose fabric incorporated lanthanide-organic framework (Ln-MOF). Dye Pigment 2018;159:491–8. https://doi.org/10.1016/j.dyepig.2018.07.026.
[23] Felgueiras HP, Tavares TD, Amorim MTP. Biodegradable, spun nanocomposite polymeric fibrous dressings loaded with bioactive biomolecules for an effective wound healing: A review. IOP Conf Ser Mater Sci Eng 2019;634:012033. https://doi.org/10.1088/1757-899X/634/1/012033.
[24] Shahnawaz Khan M, Abdelhamid HN, Wu H-F. Near infrared (NIR) laser mediated surface activation of graphene oxide nanoflakes for efficient antibacterial, antifungal and wound healing treatment. Colloids Surf B Biointerfaces 2015;127C:281–91. https://doi.org/10.1016/j.colsurfb.2014.12.049.
[25] Martina M, Hutmacher DW. Biodegradable polymers applied in tissue engineering research: a review. Polym Int 2007;56:145–57. https://doi.org/10.1002/pi.2108.
[26] Mohd Roslan MR, Mohd Kamal NL, Abdul Khalid MF, Mohd Nasir NF, Cheng EM,

Beh CY, et al. The State of Starch/Hydroxyapatite Composite Scaffold in Bone Tissue Engineering with Consideration for Dielectric Measurement as an Alternative Characterization Technique. Materials (Basel) 2021;14:1960. https://doi.org/10.3390/ma14081960.
[27] Liu S, Lin Y, Wei Y, Chen S, Zhu J, Liu L. A high performance self-healing strain sensor with synergetic networks of poly(ε-caprolactone) microspheres, graphene and silver nanowires. Compos Sci Technol 2017;146:110–8. https://doi.org/10.1016/j.compscitech.2017.03.044.
[28] Yang Y, Shen K, Lin J, Zhou Y, Liu Q, Hang C, et al. A Zn-MOF constructed from electron-rich π-conjugated ligands with an interpenetrated graphene-like net as an efficient nitroaromatic sensor. RSC Adv 2016;6:45475–81. https://doi.org/10.1039/C6RA00524A.
[29] Gopal J, Abdelhamid HN, Hua P-Y, Wu H-F. Chitosan nanomagnets for effective extraction and sensitive mass spectrometric detection of pathogenic bacterial endotoxin from human urine. J Mater Chem B 2013;1:2463. https://doi.org/10.1039/c3tb20079e.
[30] Abdelhamid HN, Wilk-Kozubek M, El-Zohry AM, Bermejo Gómez A, Valiente A, Martín-Matute B, et al. Luminescence properties of a family of lanthanide metal-organic frameworks. Microporous Mesoporous Mater 2019;279:400–6. https://doi.org/10.1016/j.micromeso.2019.01.024.
[31] Kaur D, Bharti A, Sharma T, Madhu C. Dielectric Properties of ZnO-Based Nanocomposites and Their Potential Applications. Int J Opt 2021;2021:1–20. https://doi.org/10.1155/2021/9950202.
[32] Abdelhamid HN, Mahmoud GA-E, Sharmouk W, Sharmoukh W. Correction: A cerium-based MOFzyme with multi-enzyme-like activity for the disruption and inhibition of fungal recolonization. J Mater Chem B 2020;8:7557–7557. https://doi.org/10.1039/D0TB90139C.
[33] Abdelhamid HN, Mahmoud GA-E, Sharmouk W. A cerium-based MOFzyme with multi-enzyme-like activity for the disruption and inhibition of fungal recolonization. J Mater Chem B 2020;8:7548–56. https://doi.org/10.1039/D0TB00894J.
[34] Abdelhamid HN, Badr G. Nanobiotechnology as a platform for the diagnosis of COVID-19: a review. Nanotechnol Environ Eng 2021. https://doi.org/10.1007/s41204-021-00109-0.
[35] Abdelhamid HN, Wu H-F. Multifunctional graphene magnetic nanosheet decorated with chitosan for highly sensitive detection of pathogenic bacteria. J Mater Chem B 2013;1:3950–61. https://doi.org/10.1039/c3tb20413h.
[36] Abdelhamid HN, Bermejo-Gómez A, Martín-Matute B, Zou X. A water-stable lanthanide metal-organic framework for fluorimetric detection of ferric ions and tryptophan. Microchim Acta 2017;184:3363–71. https://doi.org/10.1007/s00604-017-2306-0.
[37] Abdelhamid HN, Wu H-F. Synthesis of a highly dispersive sinapinic acid@graphene oxide (SA@GO) and its applications as a novel surface assisted laser desorption/ionization mass spectrometry for proteomics and pathogenic bacteria biosensing. Analyst 2015;140:1555–65.
[38] Abdelhamid HN, Khan MS, Wu H-FF. Design, characterization and applications of new ionic liquid matrices for multifunctional analysis of biomolecules: a novel strategy for pathogenic bacteria biosensing. Anal Chim Acta 2014;823:51–60. https://doi.org/10.1016/j.aca.2014.03.026.
[39] Abdelhamid HN, Wu H-F. Selective biosensing of Staphylococcus aureus using chitosan quantum dots. Spectrochim Acta Part A Mol Biomol Spectrosc 2018;188:50–

6. https://doi.org/10.1016/j.saa.2017.06.047.
[40] Abdelhamid HN, Wu H-F. Proteomics analysis of the mode of antibacterial action of nanoparticles and their interactions with proteins. TrAC Trends Anal Chem 2015;65:30–46. https://doi.org/10.1016/j.trac.2014.09.010.
[41] Abdelhamid HN. Nanoparticle assisted laser desorption/ionization mass spectrometry for small molecule analytes. Microchim Acta 2018;185:200. https://doi.org/10.1007/s00604-018-2687-8.
[42] Abdelhamid HN, Wu H-F. Gold nanoparticles assisted laser desorption/ionization mass spectrometry and applications: from simple molecules to intact cells. Anal Bioanal Chem 2016;408:4485–502. https://doi.org/10.1007/s00216-016-9374-6.
[43] Wu H-F, Gopal J, Abdelhamid HN, Hasan N. Quantum dot applications endowing novelty to analytical proteomics. Proteomics 2012;12:2949–61. https://doi.org/10.1002/pmic.201200295.
[44] Abdelhamid HN. Organic matrices, ionic liquids, and organic matrices@nanoparticles assisted laser desorption/ionization mass spectrometry. TrAC Trends Anal Chem 2017;89:68–98. https://doi.org/10.1016/j.trac.2017.01.012.
[45] Abdelhamid HN. Nanoparticle-based surface assisted laser desorption ionization mass spectrometry: a review. Microchim Acta 2019;186:682. https://doi.org/10.1007/s00604-019-3770-5.
[46] Abdelhamid HN, Wu H-F. Facile synthesis of nano silver ferrite (AgFeO2) modified with chitosan applied for biothiol separation. Mater Sci Eng C 2014;45:438–45. https://doi.org/10.1016/j.msec.2014.08.071.
[47] Nasser Abdelhamid H, Wu HF. Furoic and mefenamic acids as new matrices for matrix assisted laser desorption/ionization-(MALDI)-mass spectrometry. Talanta 2013;115:442–50. https://doi.org/10.1016/j.talanta.2013.05.050.
[48] Abdelhamid HN, Dowaidar M, Langel Ü. Carbonized chitosan encapsulated hierarchical porous zeolitic imidazolate frameworks nanoparticles for gene delivery. Microporous Mesoporous Mater 2020;302:110200. https://doi.org/10.1016/j.micromeso.2020.110200.
[49] Dowaidar M, Nasser Abdelhamid H, Hällbrink M, Langel Ü, Zou X. Chitosan enhances gene delivery of oligonucleotide complexes with magnetic nanoparticles–cell-penetrating peptide. J Biomater Appl 2018;33:392–401. https://doi.org/10.1177/0885328218796623.
[50] Abdel-Magied AF, Abdelhamid HN, Ashour RM, Zou X, Forsberg K. Hierarchical porous zeolitic imidazolate frameworks nanoparticles for efficient adsorption of rare-earth elements. Microporous Mesoporous Mater 2019;278:175–84. https://doi.org/10.1016/j.micromeso.2018.11.022.
[51] Abdelhamid HN, Zou X. Template-free and room temperature synthesis of hierarchical porous zeolitic imidazolate framework nanoparticles and their dye and CO2 sorption. Green Chem 2018;20:1074–84. https://doi.org/10.1039/c7gc03805d.
[52] Valencia L, Abdelhamid HN. Nanocellulose leaf-like zeolitic imidazolate framework (ZIF-L) foams for selective capture of carbon dioxide. Carbohydr Polym 2019;213:338–45. https://doi.org/10.1016/j.carbpol.2019.03.011.
[53] Abdellah AR, Abdelhamid HN, El-Adasy A-BAAM, Atalla AA, Aly KI. One-pot synthesis of hierarchical porous covalent organic frameworks and two-dimensional nanomaterials for selective removal of anionic dyes. J Environ Chem Eng 2020;8:104054. https://doi.org/10.1016/j.jece.2020.104054.
[54] Abdelhamid HN. Delafossite Nanoparticle as New Functional Materials: Advances in Energy, Nanomedicine and Environmental Applications. Mater Sci Forum 2015;832:28–53. https://doi.org/10.4028/www.scientific.net/MSF.832.28.

[55] Abdelhamid HN. High performance and ultrafast reduction of 4-nitrophenol using metal-organic frameworks. J Environ Chem Eng 2021;9:104404. https://doi.org/10.1016/j.jece.2020.104404.
[56] Kassem AA, Abdelhamid HN, Fouad DM, Ibrahim SA. Hydrogenation reduction of dyes using metal-organic framework-derived CuO@C. Microporous Mesoporous Mater 2020;305:110340. https://doi.org/10.1016/j.micromeso.2020.110340.
[57] Abdelhamid HN. Dye encapsulated hierarchical porous zeolitic imidazolate frameworks for carbon dioxide adsorption. J Environ Chem Eng 2020;8:104008. https://doi.org/10.1016/j.jece.2020.104008.
[58] Abdelhamid HN. Zinc hydroxide nitrate nanosheets conversion into hierarchical zeolitic imidazolate frameworks nanocomposite and their application for CO2 sorption. Mater Today Chem 2020;15:100222. https://doi.org/10.1016/j.mtchem.2019.100222.
[59] Kassem AA, Abdelhamid HN, Fouad DM, Ibrahim SA. Catalytic reduction of 4-nitrophenol using copper terephthalate frameworks and CuO@C composite. J Environ Chem Eng 2021;9:104401. https://doi.org/10.1016/j.jece.2020.104401.
[60] Abdelhamid HN. Hierarchical porous ZIF-8 for hydrogen production via the hydrolysis of sodium borohydride. Dalt Trans 2020;49:4416–24. https://doi.org/10.1039/D0DT00145G.
[61] Kassem AA, Abdelhamid HN, Fouad DM, Ibrahim SA. Metal-organic frameworks (MOFs) and MOFs-derived CuO@C for hydrogen generation from sodium borohydride. Int J Hydrogen Energy 2019;44:31230–8. https://doi.org/10.1016/j.ijhydene.2019.10.047.
[62] Abdelhamid HN, El-Zohry AM, Cong J, Thersleff T, Karlsson M, Kloo L, et al. Towards implementing hierarchical porous zeolitic imidazolate frameworks in dye-sensitized solar cells. R Soc Open Sci 2019;6:190723. https://doi.org/10.1098/rsos.190723.
[63] Abdelhamid HN. Zeolitic imidazolate frameworks (ZIF-8, ZIF-67, and ZIF-L) for hydrogen production. Appl Organomet Chem 2021;35:e6319. https://doi.org/https://doi.org/10.1002/aoc.6319.
[64] Abdelhamid HN, Al Kiey SA, Sharmoukh W. A high-performance hybrid supercapacitor electrode based on ZnO/nitrogen-doped carbon nanohybrid. Appl Organomet Chem 2021. https://doi.org/10.1002/aoc.6486.
[65] Abdelhamid HN, Mathew A. Cellulose-Metal Organic Frameworks (CelloMOFs) Hybrid Materials and their Multifaceted Applications: A Review. Coord Chem Rev 2022;451:214263. https://doi.org/10.1016/j.ccr.2021.214263.
[66] Goda MN, Said AE-AA, Abdelhamid HN. Highly selective dehydration of methanol over metal-organic frameworks (MOFs)-derived ZnO@Carbon. J Environ Chem Eng 2021;9:106336. https://doi.org/10.1016/j.jece.2021.106336.
[67] Abdelhamid HN. Zeolitic imidazolate frameworks (ZIF-8, ZIF-67, and ZIF-L) for hydrogen production. Appl Organomet Chem 2021;35:e6319. https://doi.org/10.1002/aoc.6319.
[68] El-Bery HM, Abdelhamid HN. Photocatalytic hydrogen generation via water splitting using ZIF-67 derived Co3O4@C/TiO2. J Environ Chem Eng 2021;9:105702. https://doi.org/10.1016/j.jece.2021.105702.
[69] Abdelhamid HN. Solid Acid Zirconium Oxo Sulfate/Carbon-Derived UiO-66 for Hydrogen Production. Energy & Fuels 2021;35:10322–6. https://doi.org/10.1021/acs.energyfuels.1c00516.
[70] Abdelhamid HN, Goda MN, Said AE-AA. Selective dehydrogenation of isopropanol on carbonized metal–organic frameworks. Nano-Structures & Nano-Objects

2020;24:100605. https://doi.org/10.1016/j.nanoso.2020.100605.
[71] Abdelhamid HN. A review on hydrogen generation from the hydrolysis of sodium borohydride. Int J Hydrogen Energy 2021;46:726–65. https://doi.org/10.1016/j.ijhydene.2020.09.186.
[72] ASTM International, D5511-18 Standard Test Method for Determining Anaerobic Biodegradation of Plastic Materials Under High-Solids Anaerobic-Digestion Conditions AI. ASTM International, D5511-18 Standard Test Method for Determining Anaerobic Biodegradation of Plastic Materials Under High-Solids Anaerobic-Digestion Conditions, ASTM International,. West Conshohocken 2018.
[73] ASASTM International, D5526-18 Standard Test Method for Determining Anaerobic Biodegradation of Plastic Materials Under Accelerated Landfill Conditions,TM International, D5526-18 Standard Test Method for Determining Anaerobic Biodegradation of Plastic Mat. ASTM International, D5526-18 Standard Test Method for Determining Anaerobic Biodegradation of Plastic Materials Under Accelerated Landfill Conditions,. ASTM Int 2018.
[74] ASTM International, D6400-19 Standard Specification for Labeling of Plastics Designed to Be Aerobically Composted in Municipal or Industrial Facilities, West Conshohocken P 2019. ASTM International, D6400-19 Standard Specification for Labeling of Plastics Designed to Be Aerobically Composted in Municipal or Industrial Facilities, West Conshohocken, PA 2019,. ASTM Int 2019.
[75] ASTM International, D6868-19 Standard Specification for Labeling of End Items That Incorporate Plastics and Polymers as Coatings or Additives with Paper and Other Substrates Designed to Be Aerobically Composted in Municipal or Industrial Facilities, W. ASTM International, D6868-19 Standard Specification for Labeling of End Items That Incorporate Plastics and Polymers as Coatings or Additives with Paper and Other Substrates Designed to Be Aerobically Composted in Municipal or Industrial Facilities, , Wes. ASTM Int 2019.
[76] Gedda G, Abdelhamid HN, Khan MS, Wu H-F. ZnO nanoparticle-modified polymethyl methacrylate-assisted dispersive liquid–liquid microextraction coupled with MALDI-MS for rapid pathogenic bacteria analysis. RSC Adv 2014;4:45973–83. https://doi.org/10.1039/C4RA03391D.
[77] Aguilar-Sanchez A, Jalvo B, Mautner A, Rissanen V, Kontturi KS, Abdelhamid HN, et al. Charged ultrafiltration membranes based on TEMPO-oxidized cellulose nanofibrils/poly(vinyl alcohol) antifouling coating. RSC Adv 2021;11:6859–68. https://doi.org/10.1039/D0RA10220B.
[78] Fijoł N, Abdelhamid HN, Pillai B, Hall SA, Thomas N, Mathew AP. 3D-printed monolithic biofilters based on a polylactic acid (PLA) – hydroxyapatite (HAp) composite for heavy metal removal from an aqueous medium. RSC Adv 2021;11:32408–18. https://doi.org/10.1039/D1RA05202K.
[79] Georgouvelas D, Abdelhamid HN, Li J, Edlund U, Mathew AP. All-cellulose functional membranes for water treatment: Adsorption of metal ions and catalytic decolorization of dyes. Carbohydr Polym 2021;264:118044. https://doi.org/10.1016/j.carbpol.2021.118044.
[80] Nasser Abdelhamid H, Mathew AP. Cellulose-zeolitic imidazolate frameworks (CelloZIFs) for multifunctional environmental remediation: Adsorption and catalytic degradation. Chem Eng J 2021;426:131733. https://doi.org/10.1016/j.cej.2021.131733.
[81] Abdelhamid HN, Mathew AP. In-situ growth of zeolitic imidazolate frameworks into a cellulosic filter paper for the reduction of 4-nitrophenol. Carbohydr Polym 2021;274:118657. https://doi.org/10.1016/j.carbpol.2021.118657.
[82] Abdelhamid HN, Mathew AP. Cellulose-Based Materials for Water Remediation:

Adsorption, Catalysis, and Antifouling. Front Chem Eng 2021;3:790314. https://doi.org/10.3389/fceng.2021.790314.
[83] Nasser Abdelhamid H, Georgouvelas D, Edlund U, Mathew AP. CelloZIFPaper: Cellulose-ZIF Hybrid Paper for Heavy Metal Removal and Electrochemical Sensing. Chem Eng J 2022:136614. https://doi.org/10.1016/j.cej.2022.136614.
[84] Abdelhamid H, Georgouvelas D, Edlund U, Mathew A. CelloZIFPaper: Cellulose-ZIF Hybrid Paper for Heavy Metal Removal and Electrochemical Sensing. ChemRxiv Cambridge Cambridge Open Engag 2022. https://doi.org/10.26434/chemrxiv-2022-gwdxf.
[85] Abdelhamid HN., Mathew AP. A Review on Cellulose-based Materials for Biomedicine. Preprints 2022:2022010035. https://doi.org/10.20944/preprints202201.0035.v1.
[86] Abdelhamid HN. Self-decontaminating antimicrobial textiles. Antimicrob. Text. from Nat. Resour., Elsevier; 2021, p. 259–94. https://doi.org/10.1016/B978-0-12-821485-5.00011-1.
[87] Abdelhamid HN, Mathew AP. Cellulose-Based Nanomaterials Advance Biomedicine: A Review. Int J Mol Sci 2022;23:5405. https://doi.org/10.3390/ijms23105405.
[88] Soliman M, Sadek AA, Abdelhamid HN, Hussein K. Graphene oxide-cellulose nanocomposite accelerates skin wound healing. Res Vet Sci 2021;137:262–73. https://doi.org/10.1016/j.rvsc.2021.05.013.
[89] Abdelhamid HN, Lin YC, Wu H-F. Thymine chitosan nanomagnets for specific preconcentration of mercury(II) prior to analysis using SELDI-MS. Microchim Acta 2017;184:1517–27. https://doi.org/10.1007/s00604-017-2125-3.
[90] Abdelhamid HN, Lin YC, Wu H-F. Magnetic nanoparticle modified chitosan for surface enhanced laser desorption/ionization mass spectrometry of surfactants. RSC Adv 2017;7:41585–92. https://doi.org/10.1039/C7RA05982E.
[91] Abdelhamid HN. Chitosan-Based Nanocarriers for Gene Delivery. Nanoeng. Biomater., Wiley; 2022, p. 91–105. https://doi.org/10.1002/9783527832095.ch4.
[92] Abdelhamid HN. Zeolitic Imidazolate Frameworks (ZIF-8) for Biomedical Applications: A Review. Curr Med Chem 2021;28:7023–75. https://doi.org/10.2174/0929867328666210608143703.
[93] Abdel-Magied AF, Abdelhamid HN, Ashour RM, Fu L, Dowaidar M, Xia W, et al. Magnetic Metal-Organic Frameworks for Efficient Removal of Cadmium(II), and Lead(II) from Aqueous Solution. J Environ Chem Eng 2022:107467. https://doi.org/10.1016/j.jece.2022.107467.
[94] Soliman AIA, Abdel-Wahab A-MA, Abdelhamid HN. Hierarchical porous zeolitic imidazolate frameworks (ZIF-8) and ZnO@N-doped carbon for selective adsorption and photocatalytic degradation of organic pollutants. RSC Adv 2022;12:7075–84. https://doi.org/10.1039/D2RA00503D.
[95] Soliman AIA, Abdelhamid HN, Aboel-Magd A. Abdel-Wahab. Hierarchical Porous Zeolitic Imidazolate Frameworks (ZIF-8) and ZnO@N-doped Carbon for Selective Adsorption and Photocatalytic Degradation of Organic Pollutants. ChemRxiv Cambridge Cambridge Open Engag 2022; 2022:10.26434/chemrxiv-2022-rwvtp. https://doi.org/10.26434/chemrxiv-2022-rwvtp.
[96] Soliman AIA, Abdel-Wahab A-MA, Abdelhamid HN. Hierarchical porous zeolitic imidazolate frameworks (ZIF-8) and ZnO@N-doped carbon for selective adsorption and photocatalytic degradation of organic pollutants. RSC Adv 2022;12:7075–84. https://doi.org/10.1039/d2ra00503d.
[97] Abdelhamid HN. A Review on Removal of Carbon Dioxide (CO2) using Zeolitic Imidazolate Frameworks: Adsorption and Conversion via Catalysis. Cambridge Open

Engag 2022. https://doi.org/10.26434/chemrxiv-2022-k23gz.
[98] Abdelhamid HN. A Review on Removal of Carbon Dioxide (CO2) using Zeolitic Imidazolate Frameworks: Adsorption and Conversion via Catalysis. Appl Organomet Chem 2022. https://doi.org/aoc.202101170.
[99] Peixoto LS, Silva FM, Niemeyer MAL, Espinosa G, Melo PA, Nele M, et al. Synthesis of Poly(Vinyl Alcohol) and/or Poly(Vinyl Acetate) Particles with Spherical Morphology and Core-Shell Structure and its Use in Vascular Embolization. Macromol Symp 2006;243:190–9. https://doi.org/10.1002/masy.200651118.
[100] Rehman MM, Siddiqui GU, Gul JZ, Kim S-W, Lim JH, Choi KH. Resistive Switching in All-Printed, Flexible and Hybrid MoS2-PVA Nanocomposite based Memristive Device Fabricated by Reverse Offset. Sci Rep 2016;6:36195. https://doi.org/10.1038/srep36195.
[101] Hmar JJL. Flexible resistive switching bistable memory devices using ZnO nanoparticles embedded in polyvinyl alcohol (PVA) matrix and poly(3,4-ethylenedioxythiophene) polystyrene sulfonate (PEDOT:PSS). RSC Adv 2018;8:20423–33. https://doi.org/10.1039/C8RA04582H.
[102] Pham NK, Vu NH, Van Pham V, Ta HKT, Cao TM, Thoai N, et al. Comprehensive resistive switching behavior of hybrid polyvinyl alcohol and TiO2 nanotube nanocomposites identified by combining experimental and density functional theory studies. J Mater Chem C 2018;6:1971–9. https://doi.org/10.1039/C7TC05140A.
[103] Koczkur KM, Mourdikoudis S, Polavarapu L, Skrabalak SE. Polyvinylpyrrolidone (PVP) in nanoparticle synthesis. Dalt Trans 2015;44:17883–905. https://doi.org/10.1039/C5DT02964C.
[104] Kumar R, Rahman H, Ranwa S, Kumar A, Kumar G. Development of cost effective metal oxide semiconductor based gas sensor over flexible chitosan/PVP blended polymeric substrate. Carbohydr Polym 2020;239:116213. https://doi.org/10.1016/j.carbpol.2020.116213.
[105] Shamsuri AA, Md. Jamil SNA, Abdan K. A Brief Review on the Influence of Ionic Liquids on the Mechanical, Thermal, and Chemical Properties of Biodegradable Polymer Composites. Polymers (Basel) 2021;13:2597. https://doi.org/10.3390/polym13162597.
[106] Ali S, Bae J, Lee CH, Choi KH, Doh YH. All-printed and highly stable organic resistive switching device based on graphene quantum dots and polyvinylpyrrolidone composite. Org Electron 2015;25:225–31. https://doi.org/10.1016/j.orgel.2015.06.040.
[107] Wang X, Yu C. Flexible low-voltage paper transistors harnessing ion gel/cellulose fiber composites. J Mater Res 2020;35:940–8. https://doi.org/10.1557/jmr.2019.303.
[108] Gaspar D, Fernandes SN, de Oliveira AG, Fernandes JG, Grey P, Pontes R V, et al. Nanocrystalline cellulose applied simultaneously as the gate dielectric and the substrate in flexible field effect transistors. Nanotechnology 2014;25:094008. https://doi.org/10.1088/0957-4484/25/9/094008.
[109] Faraji S, Danesh E, Tate DJ, Turner ML, Majewski LA. Cyanoethyl cellulose-based nanocomposite dielectric for low-voltage, solution-processed organic field-effect transistors (OFETs). J Phys D Appl Phys 2016;49:185102. https://doi.org/10.1088/0022-3727/49/18/185102.
[110] Hosseini NR, Lee J-S. Biocompatible and Flexible Chitosan-Based Resistive Switching Memory with Magnesium Electrodes. Adv Funct Mater 2015;25:5586–92. https://doi.org/10.1002/adfm.201502592.
[111] Zhang Z, Du C, Jiao H, Zhang M. Polyvinyl Alcohol/SiO2 Hybrid Dielectric for Transparent Flexible/Stretchable All-Carbon-Nanotube Thin-Film-Transistor Integration. Adv Electron Mater 2020;6:1901133.

https://doi.org/10.1002/aelm.201901133.
[112] Canimkurbey B, Çakirlar Ç, Piravadili Mucur S, Yasin M, Berber S. Influence of Al2O3 nanoparticles incorporation on the dielectric properties of solution processed PVA films for organic field effect transistor applications. J Mater Sci Mater Electron 2019;30:18384–90. https://doi.org/10.1007/s10854-019-02192-1.
[113] Midya A, Gogurla N, Ray SK. Flexible and transparent resistive switching devices using Au nanoparticles decorated reduced graphene oxide in polyvinyl alcohol matrix. Curr Appl Phys 2015;15:706–10. https://doi.org/10.1016/j.cap.2015.03.008.
[114] Xiong W, Zhu LQ, Ye C, Ren ZY, Yu F, Xiao H, et al. Flexible Poly(Vinyl Alcohol)–Graphene Oxide Hybrid Nanocomposite Based Cognitive Memristor with Pavlovian-Conditioned Reflex Activities. Adv Electron Mater 2020;6:1901402. https://doi.org/10.1002/aelm.201901402.
[115] Lockhart de la Rosa CJ, Nourbakhsh A, Heyne M, Asselberghs I, Huyghebaert C, Radu I, et al. Highly efficient and stable MoS2 FETs with reversible n-doping using a dehydrated poly(vinyl-alcohol) coating. Nanoscale 2017;9:258–65. https://doi.org/10.1039/C6NR06980K.
[116] Yu L, Zhang Y, Tong W, Shang J, Shen B, Lv F, et al. Green dielectric materials composed of natural graphite minerals and biodegradable polymer. RSC Adv 2012;2:8793. https://doi.org/10.1039/c2ra20956j.
[117] Mallick S, Ahmad Z, Touati F, Bhadra J, Shakoor RA, Al-Thani NJ. PLA-TiO2 nanocomposites: Thermal, morphological, structural, and humidity sensing properties. Ceram Int 2018;44:16507–13. https://doi.org/10.1016/j.ceramint.2018.06.068.
[118] Malakooti MH, Julé F, Sodano HA. Printed Nanocomposite Energy Harvesters with Controlled Alignment of Barium Titanate Nanowires. ACS Appl Mater Interfaces 2018;10:38359–67. https://doi.org/10.1021/acsami.8b13643.
[119] Deshmukh K, Ahamed MB, Deshmukh RR, Pasha SKK, Sadasivuni KK, Polu AR, et al. Newly developed biodegradable polymer nanocomposites of cellulose acetate and Al2O3 nanoparticles with enhanced dielectric performance for embedded passive applications. J Mater Sci Mater Electron 2017;28:973–86. https://doi.org/10.1007/s10854-016-5616-9.
[120] Nascimento M, Inácio P, Paixão T, Camacho E, Novais S, Santos T, et al. Embedded Fiber Sensors to Monitor Temperature and Strain of Polymeric Parts Fabricated by Additive Manufacturing and Reinforced with NiTi Wires. Sensors 2020;20:1122. https://doi.org/10.3390/s20041122.
[121] Bowers DT, Tanes ML, Das A, Lin Y, Keane NA, Neal RA, et al. Spatiotemporal Oxygen Sensing Using Dual Emissive Boron Dye–Polylactide Nanofibers. ACS Nano 2014;8:12080–91. https://doi.org/10.1021/nn504332j.
[122] Hammami I, Benhamou K, Hammami H, SoretoTeixeira S, Arous M, Kaddami H, et al. Electrical, morphology and structural properties of biodegradable nanocomposite polyvinyl-acetate/ cellulose nanocrystals. Mater Chem Phys 2020;240:122182. https://doi.org/10.1016/j.matchemphys.2019.122182.
[123] Ezzeddine I, Ghorbel N, Ilsouk M, Arous M, Lahcini M, Bouharras FZ, et al. Dielectric and thermal characteristics of Beidellite nanoclay-reinforced poly(butylene succinate). Mater Chem Phys 2021;258:123855. https://doi.org/10.1016/j.matchemphys.2020.123855.
[124] Choudhary S. Dielectric dispersion and relaxations in (PVA-PEO)-ZnO polymer nanocomposites. Phys B Condens Matter 2017;522:48–56. https://doi.org/10.1016/j.physb.2017.07.066.
[125] Dhatarwal P, Sengwa RJ, Choudhary S. Multifunctional (PVP/PEO)/SnO2 nanocomposites of tunable optical and dielectric properties. Optik (Stuttg)

2020;221:165368. https://doi.org/10.1016/j.ijleo.2020.165368.
[126] Abou Hammad AB, Abd El-Aziz ME, Hasanin MS, Kamel S. A novel electromagnetic biodegradable nanocomposite based on cellulose, polyaniline, and cobalt ferrite nanoparticles. Carbohydr Polym 2019;216:54–62. https://doi.org/10.1016/j.carbpol.2019.03.038.
[127] Li X, Wang J, Chen H, Xiong C, Shi Z, Yang Q. Flexible dielectric nanocomposite films based on chitin/boron nitride/copper calcium titanate with high energy density. Compos Part A Appl Sci Manuf 2021;149:106554. https://doi.org/10.1016/j.compositesa.2021.106554.
[128] Morsi MA, Asnag GM, Rajeh A, Awwad NS. Nd:YAG nanosecond laser induced growth of Au nanoparticles within CMC/PVA matrix: Multifunctional nanocomposites with tunable optical and electrical properties. Compos Commun 2021;24:100662. https://doi.org/10.1016/j.coco.2021.100662.
[129] Mohamad AH, Abdullah OG, Saeed SR. Effect of very fine nanoparticle and temperature on the electric and dielectric properties of MC-PbS polymer nanocomposite films. Results Phys 2020;16:102898. https://doi.org/10.1016/j.rinp.2019.102898.
[130] Fryń P, Lalik S, Górska N, Iwan A, Marzec M. Comparison of the Dielectric Properties of Ecoflex® with L,D-Poly(Lactic Acid) or Polycaprolactone in the Presence of SWCN or 5CB. Materials (Basel) 2021;14:1719. https://doi.org/10.3390/ma14071719.
[131] Mohammed J, Abubakar B., Yerima KU, Hamisu H, Isma'il UT, Muhammad A, et al. Biodegradable polymer modified rGO/PANI/CCTO nanocomposites: Structural and dielectric properties. Mater Today Proc 2018;5:28462–9. https://doi.org/10.1016/j.matpr.2018.10.133.
[132] Sadiq M, Hasan Raza MM, Singh AK, Chaurasia SK, Zulfequar M, Arya A, et al. Dielectric properties and ac conductivity behavior of rGO incorporated PVP-PVA blended polymer nanocomposites films. Mater Today Proc 2022;49:3164–9. https://doi.org/10.1016/j.matpr.2020.11.169.
[133] Mollik SI, Alam RB, Islam MR. Significantly improved dielectric properties of bio-compatible starch/reduced graphene oxide nanocomposites. Synth Met 2021;271:116624. https://doi.org/10.1016/j.synthmet.2020.116624.
[134] Biswas MC, Jeelani S, Rangari V. Influence of biobased silica/carbon hybrid nanoparticles on thermal and mechanical properties of biodegradable polymer films. Compos Commun 2017;4:43–53. https://doi.org/10.1016/j.coco.2017.04.005.
[135] Behera K, Chang Y-H, Yadav M, Chiu F-C. Enhanced thermal stability, toughness, and electrical conductivity of carbon nanotube-reinforced biodegradable poly(lactic acid)/poly(ethylene oxide) blend-based nanocomposites. Polymer (Guildf) 2020;186:122002. https://doi.org/10.1016/j.polymer.2019.122002.
[136] Nepomuceno NC, Seixas AAA, Medeiros ES, Mélo TJA. Evaluation of conductivity of nanostructured polyaniline/cellulose nanocrystals (PANI/CNC) obtained via in situ polymerization. J Solid State Chem 2021;302:122372. https://doi.org/10.1016/j.jssc.2021.122372.
[137] K. Algethami F, Saidi I, Ben Jannet H, Khairy M, Abdulkhair BY, Al-Ghamdi YO, et al. Chitosan-CdS Quantum Dots Biohybrid for Highly Selective Interaction with Copper(II) Ions. ACS Omega 2022. https://doi.org/10.1021/acsomega.2c01793.
[138] Abdelhamid HN, Algethami FK, Saidi I, Jannet H Ben, Khairy M, Abdulkhair BY, et al. Selective Naked-eyes Chemosensing of Cu2+ ions using Chitosan-CdS Quantum Dots Biohybrid. ChemRxiv Cambridge Cambridge Open Engag 2022; 2022. https://doi.org/10.26434/CHEMRXIV-2022-P92XT.

[139] Abdelhamid HN, El-Bery HM, Metwally AA, Elshazly M, Hathout RM. Synthesis of CdS-modified chitosan quantum dots for the drug delivery of Sesamol. Carbohydr Polym 2019;214:90–9. https://doi.org/10.1016/j.carbpol.2019.03.024.
[140] Abdelhamid HN, Wu H-F. Probing the interactions of chitosan capped CdS quantum dots with pathogenic bacteria and their biosensing application. J Mater Chem B 2013;1:6094–106. https://doi.org/10.1039/c3tb21020k.
[141] Abdelhamid HN, Wu H-F. Synthesis and multifunctional applications of quantum nanobeads for label-free and selective metal chemosensing. RSC Adv 2015;5:50494–504. https://doi.org/10.1039/C5RA07069D.
[142] Abdelhamid HN, Wu H-F. Synthesis and characterization of quantum dots for application in laser soft desorption/ionization mass spectrometry to detect labile metal–drug interactions and their antibacterial activity. RSC Adv 2015;5:76107–15. https://doi.org/10.1039/C5RA11301F.
[143] Abutalib MM, Rajeh A. Structural, thermal, optical and conductivity studies of Co/ZnO nanoparticles doped CMC polymer for solid state battery applications. Polym Test 2020;91:106803. https://doi.org/10.1016/j.polymertesting.2020.106803.
[144] Mofokeng JP, Luyt AS. Morphology and thermal degradation studies of melt-mixed poly(lactic acid) (PLA)/poly(ε-caprolactone) (PCL) biodegradable polymer blend nanocomposites with TiO2 as filler. Polym Test 2015;45:93–100. https://doi.org/10.1016/j.polymertesting.2015.05.007.
[145] Mofokeng JP, Luyt AS. Morphology and thermal degradation studies of melt-mixed PLA/PHBV biodegradable polymer blend nanocomposites with TiO 2 as filler. J Appl Polym Sci 2015;132:n/a-n/a. https://doi.org/10.1002/app.42138.
[146] Ravi M, Song S, Gu K, Tang J, Zhang Z. Electrical properties of biodegradable poly(ε-caprolactone): lithium thiocyanate complexed polymer electrolyte films. Mater Sci Eng B 2015;195:74–83. https://doi.org/10.1016/j.mseb.2015.02.003.
[147] Shen H, Li Y, Yao W, Yang S, Yang L, Pan F, et al. Solvent-free cellulose nanocrystal fluids for simultaneous enhancement of mechanical properties, thermal conductivity, moisture permeability and antibacterial properties of polylactic acid fibrous membrane. Compos Part B Eng 2021;222:109042. https://doi.org/10.1016/j.compositesb.2021.109042.
[148] Sun D, Gu T, Mao Y, Huang C, Qi X, Yang J, et al. Fabricating High-Thermal-Conductivity, High-Strength, and High-Toughness Polylactic Acid-Based Blend Composites via Constructing Multioriented Microstructures. Biomacromolecules 2022;23:1789–802. https://doi.org/10.1021/acs.biomac.2c00067.
[149] Zou Q, Xiong S, Jiang M, Chen L, Zheng K, Fu P, et al. Highly thermally conductive and eco-friendly OH-h-BN/chitosan nanocomposites by constructing a honeycomb thermal network. Carbohydr Polym 2021;266:118127. https://doi.org/10.1016/j.carbpol.2021.118127.
[150] Wang Z, Zhang T, Wang J, Yang G, Li M, Wu G. The Investigation of the Effect of Filler Sizes in 3D-BN Skeletons on Thermal Conductivity of Epoxy-Based Composites. Nanomaterials 2022;12:446. https://doi.org/10.3390/nano12030446.
[151] Fu Y, Hansson J, Liu Y, Chen S, Zehri A, Samani MK, et al. Graphene related materials for thermal management. 2D Mater 2020;7:012001. https://doi.org/10.1088/2053-1583/ab48d9.
[152] Liu Y, Wu K, Lu M, Shi J, Liang L, Lu M. Enhanced thermal conductivity of bio-based epoxy-graphite nanocomposites with degradability by facile in-situ construction of microcapsules. Compos Part B Eng 2021;218:108936. https://doi.org/10.1016/j.compositesb.2021.108936.
[153] Lu H, Xia Z, Zheng X, Mi Q, Zhang J, Zhou Y, et al. Patternable cellulose/MWCNT

laminated nanocomposites with anisotropic thermal and electrical conductivity. Compos Commun 2021;26:100786. https://doi.org/10.1016/j.coco.2021.100786.
[154] Li J, Wang Y, Yue T-N, Gao Y-N, Shi Y-D, Shen J-B, et al. Robust electromagnetic interference shielding, joule heating, thermal conductivity, and anti-dripping performances of polyoxymethylene with uniform distribution and high content of carbon-based nanofillers. Compos Sci Technol 2021;206:108681. https://doi.org/10.1016/j.compscitech.2021.108681.
[155] Guo Y, Zuo X, Xue Y, Tang J, Gouzman M, Fang Y, et al. Engineering thermally and electrically conductive biodegradable polymer nanocomposites. Compos Part B Eng 2020;189:107905. https://doi.org/10.1016/j.compositesb.2020.107905.
[156] Balogun YA, Buchanan RC. Enhanced percolative properties from partial solubility dispersion of filler phase in conducting polymer composites (CPCs). Compos Sci Technol 2010;70:892–900. https://doi.org/10.1016/j.compscitech.2010.01.009.
[157] Platnieks O, Gaidukovs S, Neibolts N, Barkane A, Gaidukova G, Thakur VK. Poly(butylene succinate) and graphene nanoplatelet–based sustainable functional nanocomposite materials: structure-properties relationship. Mater Today Chem 2020;18:100351. https://doi.org/10.1016/j.mtchem.2020.100351.
[158] Paydayesh A, Mousavi SR, Estaji S, Khonakdar HA, Nozarinya MA. Functionalized graphene nanoplatelets/poly (lactic acid)/chitosan nanocomposites: Mechanical, biodegradability, and electrical conductivity properties. Polym Compos 2022;43:411–21. https://doi.org/10.1002/pc.26385.
[159] Nezakati T, Tan A, Lim J, Cormia RD, Teoh S-H, Seifalian AM. Ultra-low percolation threshold POSS-PCL/graphene electrically conductive polymer: Neural tissue engineering nanocomposites for neurosurgery. Mater Sci Eng C 2019;104:109915. https://doi.org/10.1016/j.msec.2019.109915.
[160] Bin-Dahman OA, Rahaman M, Khastgir D, Al-Harthi MA. Electrical and dielectric properties of poly(vinyl alcohol)/starch/graphene nanocomposites. Can J Chem Eng 2018;96:903–11. https://doi.org/10.1002/cjce.22999.
[161] M. Hadi J, B. Aziz S, M. Nofal M, Hussein SA, Hafiz MH, Brza MA, et al. Electrical, Dielectric Property and Electrochemical Performances of Plasticized Silver Ion-Conducting Chitosan-Based Polymer Nanocomposites. Membranes (Basel) 2020;10:151. https://doi.org/10.3390/membranes10070151.
[162] Wu X, Jiang H, Zheng J, Wang X, Gu Z, Chen C. Highly sensitive recognition of cancer cells by electrochemical biosensor based on the interface of gold nanoparticles/polylactide nanocomposites. J Electroanal Chem 2011;656:174–8. https://doi.org/10.1016/j.jelechem.2010.11.035.
[163] Wang J, Yu J, Bai D, Li Z, Liu H, Li Y, et al. Biodegradable, Flexible, and Transparent Conducting Silver Nanowires/Polylactide Film with High Performance for Optoelectronic Devices. Polymers (Basel) 2020;12:604. https://doi.org/10.3390/polym12030604.
[164] El-Nahrawy AM, Abou Hammad AB, Khattab TA, Haroun A, Kamel S. Development of electrically conductive nanocomposites from cellulose nanowhiskers, polypyrrole and silver nanoparticles assisted with Nickel(III) oxide nanoparticles. React Funct Polym 2020;149:104533. https://doi.org/10.1016/j.reactfunctpolym.2020.104533.
[165] Patel GB, Singh NL, Singh F, Kulriya PK. Effect of swift heavy ions irradiation on physicochemical and dielectric properties of chitosan and chitosan-Ag nanocomposites. Radiat Phys Chem 2021;181:109288. https://doi.org/10.1016/j.radphyschem.2020.109288.
[166] Pan Y, Li L, Chan SH, Zhao J. Correlation between dispersion state and electrical conductivity of MWCNTs/PP composites prepared by melt blending. Compos Part A

Appl Sci Manuf 2010;41:419–26. https://doi.org/10.1016/j.compositesa.2009.11.009.
[167] Parandeh S, Kharaziha M, Karimzadeh F. An eco-friendly triboelectric hybrid nanogenerators based on graphene oxide incorporated polycaprolactone fibers and cellulose paper. Nano Energy 2019;59:412–21. https://doi.org/10.1016/j.nanoen.2019.02.058.
[168] Krucińska I, Surma B, Chrzanowski M, Skrzetuska E, Puchalski M. Application of melt-blown technology for the manufacture of temperature-sensitive nonwoven fabrics composed of polymer blends PP/PCL loaded with multiwall carbon nanotubes. J Appl Polym Sci 2013;127:869–78. https://doi.org/10.1002/app.37834.
[169] Li Y, Liu H, Dai K, Zheng G, Liu C, Chen J, et al. Tuning of vapor sensing behaviors of eco-friendly conductive polymer composites utilizing ramie fiber. Sensors Actuators B Chem 2015;221:1279–89. https://doi.org/10.1016/j.snb.2015.07.100.
[170] Rana VK, Akhtar S, Chatterjee S, Mishra S, Singh RP, Ha C-S. Chitosan and Chitosan-co-Poly(ε -caprolactone) Grafted Multiwalled Carbon Nanotube Transducers for Vapor Sensing. J Nanosci Nanotechnol 2014;14:2425–35. https://doi.org/10.1166/jnn.2014.8498.
[171] Castro M, Lu J, Bruzaud S, Kumar B, Feller J-F. Carbon nanotubes/poly(ε-caprolactone) composite vapour sensors. Carbon N Y 2009;47:1930–42. https://doi.org/10.1016/j.carbon.2009.03.037.
[172] Pötschke P, Kobashi K, Villmow T, Andres T, Paiva MC, Covas JA. Liquid sensing properties of melt processed polypropylene/poly(ε-caprolactone) blends containing multiwalled carbon nanotubes. Compos Sci Technol 2011;71:1451–60. https://doi.org/10.1016/j.compscitech.2011.05.019.
[173] Fal J, Bulanda K, Oleksy M, Sobczak J, Shi J, Liu M, et al. High AC and DC Electroconductivity of Scalable and Economic Graphite–Diamond Polylactide Nanocomposites. Materials (Basel) 2021;14:2835. https://doi.org/10.3390/ma14112835.
[174] Kashi S, Gupta RK, Baum T, Kao N, Bhattacharya SN. Dielectric properties and electromagnetic interference shielding effectiveness of graphene-based biodegradable nanocomposites. Mater Des 2016;109:68–78. https://doi.org/10.1016/j.matdes.2016.07.062.
[175] Salehi MH, Golbaten-Mofrad H, Jafari SH, Goodarzi V, Entezari M, Hashemi M, et al. Electrically conductive biocompatible composite aerogel based on nanofibrillated template of bacterial cellulose/polyaniline/nano-clay. Int J Biol Macromol 2021;173:467–80. https://doi.org/10.1016/j.ijbiomac.2021.01.121.
[176] Sownthari K, Suthanthiraraj SA. Preparation and properties of biodegradable polymer-layered silicate nanocomposite electrolytes for zinc based batteries. Electrochim Acta 2015;174:885–92. https://doi.org/10.1016/j.electacta.2015.06.049.